arXiv:1912.08822

Deconfined critical point in a doped random quantum Heisenberg magnet

Darshan G. Joshi,[1] Chenyuan Li,[1] Grigory Tarnopolsky,[1]
Antoine Georges,[2,3,4,5] and Subir Sachdev[1]

[1] *Department of Physics, Harvard University, Cambridge MA 02138, USA*
[2] *Center for Computational Quantum Physics, Flatiron Institute, New York, NY 10010 USA*
[3] *Collège de France, 11 place Marcelin Berthelot, 75005 Paris, France*
[4] *CPHT, CNRS, École Polytechnique, IP Paris, F-91128 Palaiseau, France*
[5] *DQMP, Université de Genève, 24 quai Ernest Ansermet, CH-1211 Genève, Suisse*

(Dated: February 19, 2020)

Abstract

We describe the phase diagram of electrons on a fully connected lattice with random hopping, subject to a random Heisenberg spin exchange interactions between any pair of sites and a constraint of no double occupancy. A perturbative renormalization group analysis yields a critical point with fractionalized excitations at a non-zero critical value p_c of the hole doping p away from the half-filled insulator. We compute the renormalization group to two loops, but some exponents are obtained to all loop order. We argue that the critical point p_c is flanked by confining phases: a disordered Fermi liquid with carrier density $1+p$ for $p > p_c$, and a metallic spin glass with carrier density p for $p < p_c$. Additional evidence for the critical behavior is obtained from a large M analysis of a model which extends the SU(2) spin symmetry to SU(M). We discuss the relationship of the vicinity of this deconfined quantum critical point to key aspects of cuprate phenomenology.

CONTENTS

I. INTRODUCTION

Much evidence has now accumulated for a fundamental transformation in the ground state of the cuprate superconductors near optimal hole doping $p = p_c$ [1–13]. The transformation is primarily associated with a change in the mobile carrier density from to p to $1 + p$ as p increases across p_c. There are indications of various broken symmetries for $p < p_c$, including charge and bond density waves [3, 4], spin glass order [11–13], orbital currents [9] and nematic order [4]. However, it appears that the restoration of the broken symmetry cannot be the driving mechanism for a quantum phase transition at $p = p_c$: the broken symmetries are weak and differ among the cuprates, and the transport [5], thermodynamic [6–8], electronic [2–4, 10], and spin dynamics [11–13] signatures are strong.

This paper will study a model with all-to-all randomness (see (1.1) below) which exhibits a deconfined quantum critical point [14] with many similarities to the mysterious cuprate phenomenology. Our model has a quantum critical point at $p = p_c$ with fractionalized excitations, separating metallic states with carriers densities of p and $1 + p$ (see Fig. 1). The overdoped state is a conventional disordered Fermi liquid, the underdoped 'pseudogap' phase with carrier density p has spin glass order, but the quantum critical point is described by fractionalized excitations. Our critical theory is distinct from a Landau-Hertz-Millis-type theory [15, 16] of the quantum fluctuations of the spin glass order in a metal; the latter theory has no fractionalization at criticality and does not exhibit a change in carrier density across the transition. Moreover, our $p = p_c$ critical theory is expected to maximally chaotic [17], similar to the Sachdev-Ye-Kitaev (SYK) [18, 19] models, and unlike the Landau theories [20].

Our results provide a simple rationale for the existence of a quantum phase transition in correlated metals with 'Mottness'. Broken symmetries are not essential, and only play a secondary role. At low doping, we have fermionic 'holons' of density p, moving in a background of condensed bosonic 'spinons' (see Fig. 1). At higher doping, we have condensed bosonic holons, so that the fermionic spinons behave like a Fermi liquid of hole-like carrier density $1 + p$. This statistical

transmutation, and corresponding transformation in the many-body state, is accomplished by a strongly coupled deconfined critical point which exhibits a boson-fermion duality. Note that, because of the presence of the Higgs-like condensates on both sides of the critical point, there is no true fractionalization for either $p > p_c$ or $p < p_c$.

There have been discussions [21] of deconfined critical points between a magnetic metal with 'small' Fermi surfaces, and a non-magnetic heavy Fermi liquid with a 'large' Fermi surface (a review of related ideas is in Ref. 22). However, to date, no tractable realization of this scenario has been found in non-random systems. Our results show that a similar scenario is naturally realized in models with random couplings. We also note the study of Ref 23, which found an evolution between small and large Fermi surface across optimal doping in a plaquette dynamical mean field theory.

Our model is in the class of SYK models [18, 19] with random all-to-all couplings, which have been extensively exploited recently for descriptions of strange metals and the quantum information theory of black holes. Specifically, we generalize the insulating random Heisenberg magnet originally studied in Ref. 18 to metallic states of a $t-J_{ij}$ model at non-zero doping, along the lines of Ref. 24. We consider electrons, annihilated by $c_{i\alpha}$, spin $\alpha =\uparrow,\downarrow$ on sites $i = 1 \ldots N$ with double occupancy prohibited $\sum_\alpha c^\dagger_{i\alpha} c_{i\alpha} \leq 1$. The Hamiltonian is the familiar t-J model with

$$H_{tJ} = \frac{1}{\sqrt{N}} \sum_{i\neq j=1}^{N} t_{ij} P\, c^\dagger_{i\alpha} c_{j\alpha} P + \frac{1}{\sqrt{N}} \sum_{i<j=1}^{N} J_{ij} \boldsymbol{S}_i \cdot \boldsymbol{S}_j - \mu \sum_i c^\dagger_{i\alpha} c_{i\alpha} \tag{1.1}$$

where P is the projection on non-doubly occupied sites, μ is the chemical potential and $\boldsymbol{S}_i = (1/2) c^\dagger_{i\alpha} \boldsymbol{\sigma}_{\alpha\beta} c_{i\beta}$ is the spin operator on site i, with $\boldsymbol{\sigma}$ the Pauli matrices. The complex hoppings $t_{ij} = t^*_{ji}$ and the real exchange interactions J_{ij} are independent random numbers with zero mean and mean-square values $\overline{|t_{ij}|^2} = t^2$ and $\overline{J^2_{ij}} = J^2$. We will work at a variable hole density p, defined by

$$\frac{1}{N} \sum_i \left\langle c^\dagger_{i\alpha} c_{i\alpha} \right\rangle = 1 - p\,. \tag{1.2}$$

The insulating $p = 0$ case of H_{tJ} was studied in Ref. 18, and in Ref. 24 for non-zero p, after generalizing the SU(2) spin symmetry to SU(M) and taking the large M limit (see Appendix C). A gapless critical ground state was found [18] at large M for $p = 0$. However, subsequent numerical studies [25, 26] of the insulating SU($M = 2$) case found a spin glass ground state, and such insulating spin glass states had also been examined in the large M limit [27, 28]. At non-zero p, the particular large M limit in Ref. 24 predicted a Fermi liquid ground state for all $p > 0$. We argue here that for the physical SU(2) case, the Fermi liquid only appears above a critical doping $p > p_c$, and that there is a metallic critical state very similar to the critical state of Ref. 18 at $p = p_c$. Our study was motivated by the observation of such critical spin correlations in metals in

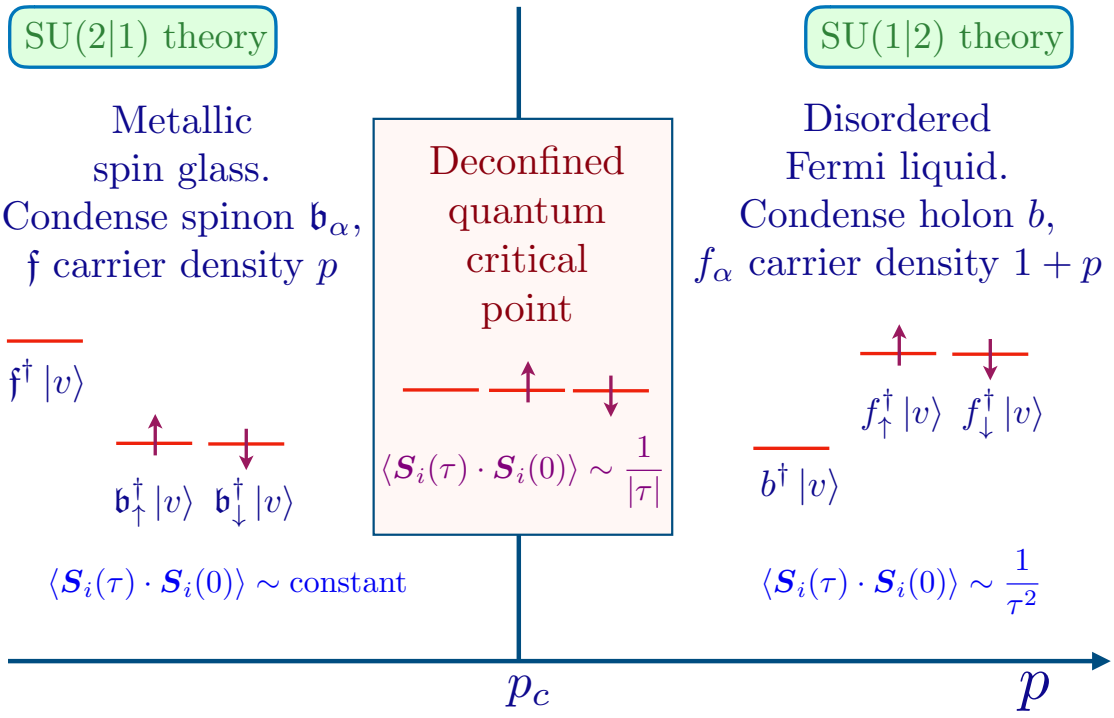

FIG. 1. Proposed phase diagram of H_{tJ} in (1.1) as function of hole doping p. The three states on each site are realized either by fermionic spinons (f_α) and bosonic holons (b) with operators as in (1.3), or by bosonic spinons ($\mathfrak{b}_\alpha$) and fermionic holons ($\mathfrak{f}$) with operators as in (1.5); $|v\rangle$ is the holon and spinon vacuum. The three states are nearly degenerate at $p = p_c$, which implies $p_c = 1/3$ at zeroth order. The critical theory can be described by both operator representations and exhibits an exact fermion-boson duality. Away from the critical point, the lower energy state is chosen to be bosonic, and that boson is condensed: so the spinons $\mathfrak{b}_\alpha$ condense for $p < p_c$, and the holons b condense for $p > p_c$. The spin correlations of SY [18], decaying as $1/|\tau|$, are realized at $p = p_c$. In the impurity model $H_{\rm imp}$ in (2.10), increasing p corresponds to increasing s_0.

numerical studies of multi-orbital Hubbard models [29, 30], and at the metal-insulator transition of a disordered Hubbard model at half-filling ($p = 0$) [31].

It is convenient to describe the 3 states on each site of the t-J model by spinon and holon operators. We can choose the spinons to be either fermions or bosons, and the holon to have the opposite statistics: the final results should be the same for all physical observables. With fermionic spinons f_α and bosonic holons b, the 3 physical states are $f^\dagger_\alpha|v\rangle$ and $b^\dagger|v\rangle$ (where $|v\rangle$ is the spinon and holon vacuum, and we drop site indices), see Fig. 1. Then the operators

$$c_\alpha = b^\dagger f_\alpha \quad , \quad \boldsymbol{S} = \frac{1}{2} f^\dagger_\alpha \boldsymbol{\sigma}_{\alpha\beta} f_\beta \quad , \quad V = b^\dagger b + \frac{1}{2} f^\dagger_\alpha f_\alpha \tag{1.3}$$

are all physical observables which realize the superalgebra SU(1|2) [32] (see Appendix A). We are interested in the 3-dimensional representation of physical states obeying

$$f_\alpha^\dagger f_\alpha + b^\dagger b = 1\,; \tag{1.4}$$

Hence, the physical states are invariant under the U(1) gauge transformation $f_\alpha \to f_\alpha e^{i\phi}$, $b \to b e^{i\phi}$, while individual spinon and holon excitations carry U(1) gauge charges.

Alternatively we can use a representation with bosonic spinons $\mathfrak{b}_\alpha$ and fermionic holons $\mathfrak{f}$. Now the gauge-invariant operators are

$$c_\alpha = \mathfrak{f}^\dagger \mathfrak{b}_\alpha \quad , \quad \boldsymbol{S} = \frac{1}{2}\mathfrak{b}_\alpha^\dagger \boldsymbol{\sigma}_{\alpha\beta} \mathfrak{b}_\beta \quad , \quad V = \mathfrak{f}^\dagger \mathfrak{f} + \frac{1}{2}\mathfrak{b}_\alpha^\dagger \mathfrak{b}_\alpha\,. \tag{1.5}$$

This realizes the same superalgebra SU(2|1) $\equiv$ SU(1|2) as (1.3), and the same 3-dimensional representation is obtained by the constraint

$$\mathfrak{b}_\alpha^\dagger \mathfrak{b}_\alpha + \mathfrak{f}^\dagger \mathfrak{f} = 1\,. \tag{1.6}$$

Note that while we find it convenient to refer to the superalgebra, there will be no supersymmetry in our results: H_{tJ} does not commute with all SU(1|2) generators.

We can now describe the structure of our main results illustrated in Fig. 1. We find a deconfined critical point $p = p_c$ at which the 3 spinon and holon states are nearly degenerate. Assuming all three states are equally probable at criticality, we obtain a critical density $p_c = 1/3$. Indeed, $p_c = 1/3$ is the zeroth order result of our renormalization group (RG) analysis, as we show in Appendix D 2; however, there are non-universal higher order corrections to the value of p_c. We can formulate this critical theory using *either* of the representations in (1.3) and (1.5). This exact fermion-boson duality is an elementary analog of the fermion-boson duality of 2+1 dimensional field theories describing the deconfined critical point of the square lattice antiferromagnet [33, 34]; as in the 2+1 dimensional theories, we will find that a Wess-Zumino-Witten [32, 35–38] term ($\mathcal{S}_B$ in (2.4) and (2.6) below) plays a central role in the criticality.

Away from the critical point, there is a runaway RG flow to states in which either the spinon or holon states are lower in energy. As illustrated in Fig. 1, we argue that this RG flow implies that we should now *choose* between the representations in (1.3) and (1.5) so that the lower energy state is a boson, and we should condense that boson. For $p > p_c$, the holon states are lower in energy; so we should choose (1.3) and condense b—this breaks the U(1) gauge symmetry, and we obtain a disordered Fermi liquid in which the f_α behave like electrons of density $1 - p$ (which is the same as holes of density $1 + p$ for the underlying Hubbard model). Conversely, for $p < p_c$, the spinon states are lower in energy; so we should choose (1.5) and condense $\mathfrak{b}_\alpha$—this again breaks the U(1) gauge symmetry, and we obtain a metallic spin glass in which the $\mathfrak{f}$ behave like holes of density p. Note that as $p \to 0$, this metallic spin glass becomes the insulating spin glass found

in earlier studies [25–28]. The large-M limit considered in Ref. 24 captures the disordered Fermi liquid, but does not capture the metallic spin-glass phase and the deconfined critical point at a non-zero $p = p_c$.

We will describe the nature of the infinite volume ($N \to \infty$) limit of H_{tJ} in Section II, and map possible critical states of the large N limit to quantum impurity models in Section II A. The RG analysis of the impurity model appears in Section III, where we obtain critical exponents of the deconfined critical point to two-loop order; the anomlaous dimensions of the electron and spin operators are obtained to all-loop order. We turn to the phases flanking the critical point in Section IV, and summarize our results in Section V. The appendices contain various technical details; in particular, the RG equations for a generalized model with SU(M) spin symmetry appear in Appendix B, and the large M analysis appears in Appendix C.

II. LARGE VOLUME LIMIT

The limit of large volume ($N \to \infty$) of H_{tJ} is obtained by the methods described in Refs. [18, 27, 28] for the insulating model at $p = 0$. We introduce field replicas in the path integral, and average over t_{ij} and J_{ij}. At the $N = \infty$ saddle point, the problem reduces to a single site problem, with the fields carrying replica indices. The replica structure is important in the spin glass phase [27, 28], which we will explore in subsequent work. In the interests of simplicity, we drop the replica indices here as they play no significant role in the critical theory and the RG equations. Within the imaginary time path integral formalism (with $\tau \in [0, 1/T]$, with T the temperature), the solution of the model involves a local single-site effective action which reads:

$$\begin{aligned} \mathcal{Z} &= \int \mathcal{D}c_\alpha(\tau) e^{-\mathcal{S}-\mathcal{S}_\infty} \\ \mathcal{S} &= \int d\tau \left[c_\alpha^\dagger(\tau) \left(\frac{\partial}{\partial \tau} - \mu \right) c_\alpha(\tau) \right] + t^2 \int d\tau d\tau' R(\tau - \tau') c_\alpha^\dagger(\tau) c_\alpha(\tau') \\ &\quad - \frac{J^2}{2} \int d\tau d\tau' Q(\tau - \tau') \boldsymbol{S}(\tau) \cdot \boldsymbol{S}(\tau') \,, \end{aligned} \tag{2.1}$$

In this expression, μ is the chemical potential determined to satisfy (1.2) and $\mathcal{S}_\infty$ is the action associated with the constraint of no double occupancy ($U = \infty$). Decoupling the path integral introduces fields analogous to R and Q which are initially off-diagonal in the spin SU(2) indices. We have assumed above that the large-volume limit is dominated by the saddle point in which spin rotation symmetry is preserved on the average, and so R and Q were taken to diagonal in spin indices. The path integral $\mathcal{Z}$ is a functional of the fields $R(\tau)$ and $Q(\tau)$, and we define its

correlators

$$\overline{R}(\tau-\tau') = -\left\langle c_\alpha(\tau) c_\alpha^\dagger(\tau')\right\rangle_{\mathcal{Z}}$$
$$\overline{Q}(\tau-\tau') = \frac{1}{3}\left\langle \boldsymbol{S}(\tau)\cdot\boldsymbol{S}(\tau')\right\rangle_{\mathcal{Z}} \tag{2.2}$$

In the thermodynamic ($N\to\infty$) limit, the solution of the model is obtained by imposing the two self-consistency conditions:

$$R(\tau) = \overline{R}(\tau) \quad , \quad Q(\tau) = \overline{Q}(\tau). \tag{2.3}$$

These equations and the mapping to a local effective action are part of the extended dynamical mean-field theory framework (EDMFT), which becomes exact for random models on fully connected lattices [16]. They can also be viewed as an EDMFT approximation to the non-random t-J model [23, 39–41]. To make contact with notations often used in the (E)DMFT literature, we note that $t^2R(\tau-\tau')$ is the self-consistent 'hybridization function' (dynamical mean-field) $\Delta(\tau-\tau')$.

This path-integral representation can be formulated in the SU(1|2) representation (1.3) as:

$$\begin{aligned}
\mathcal{Z} &= \int \mathcal{D}f_\alpha(\tau)\mathcal{D}b(\tau)\mathcal{D}\lambda(\tau) e^{-\mathcal{S}_B-\mathcal{S}_{tJ}} \\
\mathcal{S}_B &= \int d\tau \left[f_\alpha^\dagger(\tau)\frac{\partial}{\partial\tau} f_\alpha(\tau) + b^\dagger(\tau)\frac{\partial}{\partial\tau} b(\tau) + i\lambda(\tau)\left(f_\alpha^\dagger(\tau) f_\alpha(\tau) + b^\dagger(\tau) b(\tau) - 1\right)\right] \\
\mathcal{S}_{tJ} &= \int d\tau\, s_0\, f_\alpha^\dagger(\tau) f_\alpha(\tau) + t^2 \int d\tau d\tau' R(\tau-\tau') f_\alpha^\dagger(\tau) b(\tau) b^\dagger(\tau') f_\alpha(\tau') \\
&\quad - \frac{J^2}{2}\int d\tau d\tau' Q(\tau-\tau')\boldsymbol{S}(\tau)\cdot\boldsymbol{S}(\tau')\,,
\end{aligned} \tag{2.4}$$

where $\boldsymbol{S}(\tau)$ is to be represented by (1.3). Here $\mathcal{S}_B$ is the kinematic Berry phase (*i.e.* the Wess-Zumino-Witten term [35]) of the SU(1|2) superspin at each site [32], $\mathcal{S}_{tJ}$ is the action containing the terms arising from H_{tJ}, λ is the Lagrange multiplier imposing Eq. (1.4) and the chemical potential s_0 is determined to satisfy (1.2), which now becomes

$$\left\langle b^\dagger b\right\rangle_{\mathcal{Z}} = p\,. \tag{2.5}$$

Note that $\mathcal{Z}$ is a U(1) gauge theory, and under the U(1) gauge transformation $\lambda\to\lambda-\partial_\tau\phi$.

Let us also present the exactly equivalent formulation of the large N saddle point in terms of the SU(2|1) superspin. Now the Berry phase $\mathcal{S}_B$ in (2.4) is replaced by

$$\mathcal{S}_B = \int d\tau \left[\mathfrak{b}_\alpha^\dagger(\tau)\frac{\partial}{\partial\tau}\mathfrak{b}_\alpha(\tau) + \mathfrak{f}^\dagger(\tau)\frac{\partial}{\partial\tau}\mathfrak{f}(\tau) + i\lambda(\tau)\left(\mathfrak{b}_\alpha^\dagger(\tau)\mathfrak{b}_\alpha(\tau) + \mathfrak{f}^\dagger(\tau)\mathfrak{f}(\tau) - 1\right)\right], \tag{2.6}$$

while $\mathcal{S}_{tJ}$ has the same form, apart from representing $c_\alpha(\tau)$ and $\boldsymbol{S}(\tau)$ by (1.5), and replacing the s_0 term by $s_0\mathfrak{b}_\alpha^\dagger(\tau)\mathfrak{b}_\alpha(\tau)$. The density constraint determining s_0 in (2.5) is replaced by

$$\left\langle \mathfrak{f}^\dagger\mathfrak{f}\right\rangle_{\mathcal{Z}} = p\,. \tag{2.7}$$

Appendix C analyzes the path integral (2.4) using a large M expansion in an approach which generalizes the SU(2) spin symmetry to SU(M); a similar large M method has been used previously for a Hubbard model [42–44] and other phases of a disordered t-J model [45].

The body of the paper will focus on an RG analysis of $\mathcal{Z}$. This is performed by expressing it in terms of an auxiliary quantum impurity problem, which we will now set up.

A. Mapping to a quantum impurity problem

In our RG analysis, we find it useful to consider the path integral as a functional of the fields $R(\tau)$ and $Q(\tau)$ with an arbitrary time dependence, and to defer imposition of the self-consistency conditions in (2.3). As we are looking for critical states, we assume that these fields have a power-law decay in time with

$$Q(\tau) \sim \frac{1}{|\tau|^{d-1}} \quad , \quad R(\tau) \sim \frac{\mathrm{sgn}(\tau)}{|\tau|^{r+1}} \, . \tag{2.8}$$

where, for now, d and r are arbitrary numbers determining exponents, which will only be determined after imposing (2.3). Our analysis exploits the freedom to choose d and r: we will show that a systematic RG analysis of the path integral $\mathcal{Z}$ is possible to all orders in ϵ and $\bar{r}$, where

$$\epsilon = 3 - d \quad , \quad \bar{r} = \frac{1-r}{2} \; ; \; Q(\tau) \sim \frac{1}{|\tau|^{2-\epsilon}} \quad , \quad R(\tau) \sim \frac{\mathrm{sgn}(\tau)}{|\tau|^{2-2\bar{r}}} \, . \tag{2.9}$$

The analysis assumes ϵ and $\bar{r}$ are of the same order, and expands order-by-order in homogeneous polynomials in ϵ and $\bar{r}$. Such RG analyses were carried out in Refs. [46–48] for an insulating spin model in which $t = 0$, and by Fritz and Vojta [49–51] for a pseudogap Anderson impurity model in which $J = 0$ (see also Refs. [52, 53]); we note that the $\bar{r}$ expansion of Refs. [49–51] was in good agreement with numerical studies [54]. We will combine these analyses here, and our notations here for ϵ and $\bar{r}$ follow these earlier works.

We proceed by decoupling the last two terms in $\mathcal{S}$ by introducing fermionic (ψ_α) and bosonic (ϕ_a, $a = x, y, z$) fields respectively, and then the path integral $\mathcal{Z}$ reduces to a quantum impurity problem. The 'impurity' is a SU(1|2) superspin realizing the 3 states on each site of the t-J model, and this is coupled to a 'superbath' of the ψ_α and ϕ_a excitations. The quantum impurity problem is specified by the Hamiltonian

$$\begin{aligned} H_{\mathrm{imp}} = & \, (s_0 + \lambda) f_\alpha^\dagger f_\alpha + \lambda \, b^\dagger b + g_0 \left(f_\alpha^\dagger b \, \psi_\alpha(0) + \mathrm{H.c.} \right) + \gamma_0 f_\alpha^\dagger \frac{\sigma^a_{\alpha\beta}}{2} f_\beta \, \phi_a(0) \\ & + \int |k|^r dk \, k \, \psi^\dagger_{k\alpha} \psi_{k\alpha} + \frac{1}{2} \int d^d x \left[\pi_a^2 + (\partial_x \phi_a)^2 \right] \, . \end{aligned} \tag{2.10}$$

For completeness let us also explicitly present the Hamiltonian using a SU(2|1) impurity of bosonic spinons and fermionic holons

$$H_{\rm imp} = (s_0+\lambda)\mathfrak{b}_\alpha^\dagger \mathfrak{b}_\alpha + \lambda\, \mathfrak{f}^\dagger \mathfrak{f} + g_0 \left(\mathfrak{b}_\alpha^\dagger \mathfrak{f}\, \psi_\alpha(0) + \text{H.c.}\right) + \gamma_0 \mathfrak{b}_\alpha^\dagger \frac{\sigma^a_{\alpha\beta}}{2} \mathfrak{b}_\beta\, \phi_a(0) + \int |k|^r dk\, k\, \psi_{k\alpha}^\dagger \psi_{k\alpha} + \frac{1}{2}\int d^d x \left[\pi_a^2 + (\partial_x \phi_a)^2\right] . \tag{2.11}$$

We note several features of $H_{\rm imp}$, which apply equally to (2.10) and (2.11):

- The bosonic bath is realized by a free massless scalar field in d spatial dimensions, as in Refs. [46–48]. The field π_a is canonically conjugate to the field ϕ_a. The impurity spin $\boldsymbol{S}$ couples to the value of ϕ_a at the spatial origin, $\phi_a(0) \equiv \phi_a(x=0,\tau)$. It is easy to verify that upon integrating out ϕ_a from $H_{\rm imp}$, we obtain the J term in $\mathcal{S}_{tJ}$, with $Q(\tau)$ obeying (2.8).

- The fermionic bath is realized by free fermions $\psi_{k\alpha}$ with energy k and a 'pseudogap' density of states $\sim |k|^r$. The impurity electron operator c_α is coupled to $\psi_\alpha(0) \equiv \int |k|^r dk\, \psi_{k\alpha}$. Integrating out $\psi_{k\alpha}$ from $H_{\rm imp}$ yields the t term in $\mathcal{S}_{tJ}$, with $R(\tau)$ obeying (2.8).

- We have replaced the path integral over the Lagrange multiplier $i\lambda$ in $\mathcal{S}_B$ by a constant real λ. The constraint (1.4) can be conveniently and exactly imposed by the Abrikosov method of sending $\lambda \to \infty$ [48–51], as we will see in Section III. So the consequences of $\mathcal{S}_B$ will be accounted for exactly, and that is also the case for the alternative analysis in Appendix B, where $\mathcal{S}_B$ is accounted for by the exact implementation of the superalgebras.

- The two formulations of $H_{\rm imp}$ in (2.10) and (2.11) are equivalent, and lead to identical RG equations. This is because, ultimately, the quantum dynamics depends only upon the superspin algebra and the representation of the superspin on each site, and these are the same for SU(2|1) formulation by (1.3,1.4) and SU(1|2) formulation by (1.5,1.6). An explicit derivation of the one-loop RG equations using only the superspin algebra and representation appears in Appendix B.

- The model is now characterized by 3 couplings constants, s_0, γ_0, and g_0, we will derive the RG equations for these couplings in Section III. The coupling of the superspin to the fermionic bath is g_0, and to the bosonic bath is γ_0: we will see that the RG flow of these couplings is marginal for small ϵ and $\bar{r}$, and they are attracted to a deconfined critical point.

- The coupling s_0 acts like a 'Zeeman field' on the superspin, which breaks the degeneracy between the spinon and holon states. The flow of s_0 is strongly relevant at the deconfined critical point, and this drives the system into one of the two phases in Fig. 1.

We note that impurity models with both fermionic and bosonic baths have been considered earlier by Sengupta [55], and by Si and collaborators [56–58], but not for the 'superspin' case with significant particle-hole asymmetric charge fluctuations on the impurity site. Specifically, we fully project out doubly occupied states, while keeping holon states low energy, and these features are crucial to the structure of our critical theory, as in Refs. [49–51]. Also, the effect of a Zeeman field in an impurity spin model with a bosonic environment was studied in Refs. [59–61] in the context of the superfluid-insulator transition.

III. RG ANALYSIS

This section will present the RG analysis of the impurity model defined by (2.10). The RG analysis will initially not account for the self-consistency conditions (2.3). We will apply them later in Section III E.

We will employ the SU(1|2) superspin formulation, although essentially the same analysis can be applied to the SU(2|1) superspin, with exactly the same results. A key feature of the computation is that we impose the local constraint (1.4) exactly. This implemented by the Abrikosov method of taking the $\lambda \to \infty$ limit, as described in earlier analyses [48–51].

An alternative approach to obtain the RG equations generalizes the method of Refs. [46, 47] for SU(2) spins to superspins in either SU(2|1) or SU(1|2). This method utilizes only gauge-invariant information contained in the superspin algebra and its representation, and is presented in Appendix B. The RG equations are identical to those obtained in this section.

At the tree-level, we can identify the scaling dimensions from (2.10):

$$\begin{aligned} &\mathrm{dim}[f] = \mathrm{dim}[b] = 0\,, \quad \mathrm{dim}[\psi_{k\alpha}] = -\frac{1+r}{2} = -\mathrm{dim}[\psi_\alpha(0)]\,, \\ &\mathrm{dim}[g_0] = \frac{1-r}{2} \equiv \bar{r}\,, \quad \mathrm{dim}[\gamma_0] = \frac{3-d}{2} \equiv \frac{\epsilon}{2}\,, \quad \mathrm{dim}[\phi_a] = \frac{d-1}{2}\,. \end{aligned} \tag{3.1}$$

This establishes $r = 1$ and $d = 3$ as upper critical dimensions.

We define the following renormalized fields and couplings,

$$f_\alpha = \sqrt{Z_f} f_{R\alpha}\,, \quad b = \sqrt{Z_b} b_R\,, \quad g_0 = \frac{\mu^{\bar{r}} Z_g}{\sqrt{Z_f Z_b}} g\,, \quad \gamma_0 = \frac{\mu^{\epsilon/2} Z_\gamma}{Z_f \sqrt{Z_\phi \widetilde{S}_{d+1}}} \gamma\,, \quad \phi_a = \sqrt{Z_\phi}\phi_{Ra}\,, \tag{3.2}$$

where $\widetilde{S}_d = \Gamma(d/2-1)/(4\pi^{d/2})$. The renormalization factors are to be obtained from self-energy and vertex corrections, as we will show below. We will work with $s_0 = 0$ and subsequently derive the flow away from it. Also, we work at zero temperature, i.e., $\beta \to \infty$.

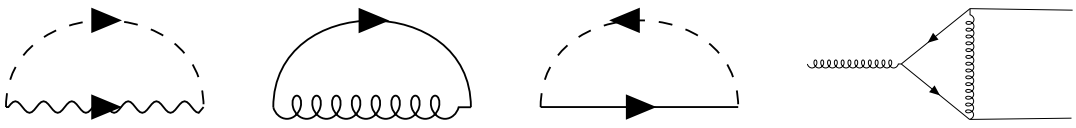

(a) (b) (c) (d)

FIG. 2. One-loop diagrams for self energy and vertex corrections. Fermion self-energy diagrams are shown in (a) and (b), boson self energy is shown in (c), and γ_0 vertex correction is shown in (d). In these diagrams, solid line is for f propagator, dashed line is for ψ propagator, wavy is for b propagator, and spiral is for ϕ propagator.

A. Fermion and boson self energy

Interaction terms in our action lead to self-energy corrections to the fermion and boson propagator. The corresponding Feynman diagrams at one-loop level are shown in Fig. 2 (a)-(c), while Feynman diagrams for self-energy to two-loop order are shown in Figs. 10 and 11. Here we show explicit result for one-loop diagrams and refer to Appendix D for details regarding two-loop calculations.

We first calculate the fermionic self energy at one-loop level. At this level there are no diagrams which mixes the vertices corresponding to the bosonic bath coupling and the fermionic bath coupling. Here we have two relevant diagrams and we quote the self-energy below:

$$\begin{aligned}\Sigma^f_{2(a)} &= -g_0^2\frac{1}{\beta}\sum_{i\omega_n}\int_{-\infty}^{\infty}dk\frac{|k|^r}{i\omega_n-k}\frac{1}{i\nu-i\omega_n-\lambda} = g_0^2\int_{-\infty}^{\infty}dk\frac{|k|^r\theta(k)}{i\nu-\lambda-k} \qquad \text{(Recall } \lambda\to\infty\text{)}\\ &= g_0^2\pi\csc(\pi r)(\lambda-i\nu)^r = A_\mu(i\nu-\lambda)g^2\left[-\frac{1}{2\bar{r}}+i\pi\right] \qquad , \qquad (3.3)\\ \Sigma^f_{2(b)} &= \gamma_0^2\frac{3}{4}\frac{1}{\beta}\sum_{i\omega_n}\int\frac{d^dk}{(2\pi)^d}\frac{1}{\omega_n^2+k^2}\frac{1}{i\nu+i\omega_n-\lambda} = \gamma_0^2\frac{3}{4}\frac{S_d}{2}\int_0^{\infty}dk\frac{k^{d-2}}{i\nu-\lambda-k}\\ &= \gamma_0^2\frac{3}{4}\frac{S_d}{2}\pi\csc(\pi(d-2))(\lambda-i\nu)^{-2+d} = B_\mu\frac{3}{4}\gamma^2(i\nu-\lambda)\left[-\frac{1}{\epsilon}+\frac{1}{2}(\aleph+2i\pi)\right], \qquad (3.4)\end{aligned}$$

where we wrote $\int d^dk/(2\pi)^d = S_d\int dkk^{d-1}$, $S_d = 2/(\Gamma(d/2)(4\pi)^{d/2})$,

$$A_\mu = \mu^{2\bar{r}}(i\nu-\lambda)^{-2\bar{r}}\frac{Z_g^2}{Z_fZ_b}, \qquad (3.5)$$

$$B_\mu = \mu^{\epsilon}(i\nu-\lambda)^{-\epsilon}\frac{Z_\gamma^2}{Z_f^2Z_\phi}, \qquad (3.6)$$

$$\aleph = 2(\gamma_E-1) = -0.845569\ldots, \qquad (3.7)$$

with γ_E being the Euler's constant.

For the bosonic self energy there is only one diagram (Fig. 2(c)) at the one-loop level. The self energy is evaluated as follows:

$$\Sigma^b_{2(c)} = 2g_0^2 \frac{1}{\beta} \sum_{i\omega_n} \int_{-\infty}^{\infty} dk \frac{|k|^r}{i\omega_n - k} \frac{1}{i\nu + i\omega_n - \lambda} = g_0^2 \int_{-\infty}^{\infty} dk \frac{|k|^r \theta(k)}{i\nu - \lambda - k} \qquad \text{(Recall } \lambda \to \infty\text{)}$$
$$= 2g_0^2 \pi \csc(\pi r)(\lambda - i\nu)^r = A_\mu (i\nu - \lambda) 2g^2 \left[-\frac{1}{2\bar{r}} + i\pi \right] . \qquad (3.8)$$

A factor of 2 is due to the spin index of internal f and ψ-line.

The expressions for $\Sigma^f_{2(a)}$ and $\Sigma^f_{2(c)}$ agree with those in Refs. [49–51], while that for $\Sigma^f_{2(b)}$ agrees with that in Ref. 48. Similarly, the self-energy diagrams at two-loop level are evaluated in a straightforward manner, as shown in Appendix D.

B. Vertex correction

There is no one-loop vertex correction to the fermionic bath coupling g_0. However, it does acquire corrections at two-loop level and the corresponding diagrams are shown in Fig. 12. The bosonic bath coupling γ_0 has vertex corrections both at the one-loop and two-loop level. The one-loop diagram is shown in Fig. 2(d), while the two-loop diagrams are shown in Fig. 13. Here we explicitly evaluated the one-loop vertex correction to γ_0,

$$\Gamma^\gamma_{2(d)} = (-\frac{1}{4})\gamma_0^3 \frac{1}{\beta} \sum_{i\omega_{1n}} \int \frac{d^d k_1}{(2\pi)^d} \frac{1}{\omega_{1n}^2 + k_1^2} \frac{1}{i\Omega_{1n} + i\omega_{1n} - \lambda} \frac{1}{i\Omega_{2n} + i\omega_{1n} - \lambda}$$
$$= (-\frac{1}{4})\gamma_0^3 \int \frac{d^d k_1}{(2\pi)^d} \frac{1}{2k_1} \frac{1}{i\Omega_{1n} - k_1 - \lambda} \frac{1}{i\Omega_{2n} - k_1 - \lambda}$$
$$= -\gamma_0 B_\mu \gamma^2 \frac{1}{4} \left[\frac{1}{\epsilon} - 1 + \frac{1}{2}(-\aleph - 2i\pi) \right] . \qquad (3.9)$$

This expression agrees with that in Ref. 48. We can similarly evaluate the two-loop level corrections and these are quoted in the Appendix D.

C. Beta functions and fixed points

We now demand the cancellation of poles in the expression for the renormalized vertex and the f/b Green's functions at the external frequency, $i\nu - \lambda = \mu$. This leads to the following expressions of the renormalization factors. Note that $Z_\phi = 1$ exactly, owing to the absence of bulk interaction

terms such as ϕ^4. For the rest we have,

$$Z_f = 1 - \frac{g^2}{2\bar{r}} - \frac{3\gamma^2}{4\epsilon} - \frac{15\gamma^4}{32\epsilon^2} + \frac{3\gamma^4}{8\epsilon} - \frac{g^4}{4\bar{r}^2} + \frac{g^4}{2\bar{r}} - \frac{3g^2\gamma^2}{8\epsilon\bar{r}} + \frac{3g^2\gamma^2}{8\bar{r}(\epsilon+2\bar{r})} + \frac{3g^2\gamma^2(2+\aleph)}{8(\epsilon+2\bar{r})}\,, \tag{3.10}$$

$$Z_b = 1 - \frac{g^2}{\bar{r}} - \frac{g^4}{4\bar{r}^2} + \frac{g^4}{2\bar{r}} - \frac{3g^2\gamma^2}{4\epsilon\bar{r}} + \frac{3g^2\gamma^2}{2\epsilon(\epsilon+2\bar{r})} + \frac{3(2-\aleph)g^2\gamma^2}{4(\epsilon+2\bar{r})}\,, \tag{3.11}$$

$$Z_g = 1 + \frac{g^4}{4\bar{r}}\,, \tag{3.12}$$

$$Z_\gamma = 1 + \frac{\gamma^2}{4\epsilon} + \frac{9\gamma^4}{32\epsilon^2} - \frac{\gamma^4}{8\epsilon} + \frac{g^2\gamma^2}{4\epsilon\bar{r}} - \frac{g^2\gamma^2}{4\bar{r}(\epsilon+2\bar{r})} - \frac{g^2\gamma^2\aleph}{4(\epsilon+2\bar{r})}\,. \tag{3.13}$$

Using Eqns. (D3) and (D4), we obtain the beta functions as follows:

$$\beta(g) = -\bar{r}g + \frac{3}{2}g^3 + \frac{3}{8}g\gamma^2 - g^5 + \frac{3}{16}g^3\gamma^2\aleph - \frac{9}{8}g^3\gamma^2 - \frac{3}{8}g\gamma^4 \tag{3.14}$$

$$\beta(\gamma) = -\frac{\epsilon}{2}\gamma + \gamma^3 + g^2\gamma - \gamma^5 - \frac{5}{8}g^2\gamma^3\aleph - \frac{3}{4}g^2\gamma^3 - 2g^4\gamma \tag{3.15}$$

We can find the fixed points to two-loop order by setting the beta functions to zero. This gives us four fixed points $(g*^2, \gamma*^2)$:

$$FP_1 = (0,0)\,, \tag{3.16}$$

$$FP_2 = \left(0, \frac{\epsilon}{2} + \frac{\epsilon^2}{4}\right)\,, \tag{3.17}$$

$$FP_3 = \left(\frac{2\bar{r}}{3} + \frac{8}{27}\bar{r}^2, 0\right)\,, \tag{3.18}$$

$$FP_4 = \left(-\frac{\epsilon}{6} + \frac{8\bar{r}}{9} + \epsilon^2\left[-\frac{25}{324} + \frac{\aleph}{24}\right] + \bar{r}^2\left[-\frac{304}{729} + \frac{8\aleph}{27}\right] + \epsilon\bar{r}\left[\frac{119}{243} - \frac{5\aleph}{18}\right],\right.$$
$$\left.\frac{2\epsilon}{3} - \frac{8\bar{r}}{9} + \epsilon^2\left[\frac{40}{81} - \frac{\aleph}{9}\right] + \bar{r}^2\left[\frac{1600}{729} - \frac{64\aleph}{81}\right] + \epsilon\bar{r}\left[-\frac{416}{243} + \frac{20\aleph}{27}\right]\right)\,. \tag{3.19}$$

The stability of the fixed points can be analyzed by looking at the eigenvalues of the stability matrix. We find that the Gaussian fixed point is always unstable. Importantly, we find that the non-trivial fixed point, FP_4, with $g* \neq 0$ and $\gamma* \neq 0$ is stable for a range of values in the parameter space of ϵ and $\bar{r}$. In Fig. 3 we plot the RG flow in the $g-\gamma$ plane at one-loop level and show the different fixed points.

These fixed points corresponds to the underlying t-J model at a non-zero doping density p. However, the precise value of p depends upon high energy details, and cannot be deduced from the fixed point couplings, as we discuss in Appendix D 2.

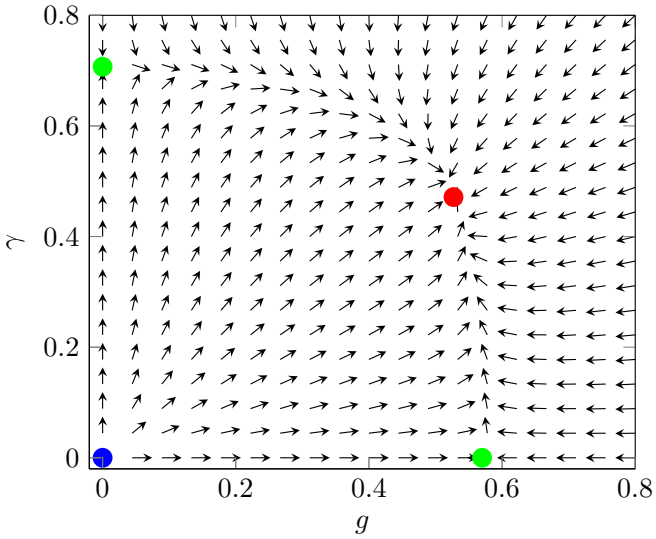

FIG. 3. One loop RG flow in the $g-\gamma$ plane plotted for $\epsilon = 1$ and $\bar{r} = 0.5$. The red point is the stable fixed point (FP_4), green points are the saddle (FP_2 and FP_3) and blue point is the unstable Gaussian fixed point (FP_1). Note that the flow in the s direction is always relevant (not shown).

D. Anomalous dimensions of f_α and b

With the beta function at hand, it is straight forward to calculate the anomalous dimension of the fermion and boson propagators, defined as follows:

$$\eta_f = \mu \frac{d \ln Z_f}{d\mu}\bigg|_{FP} , \qquad \eta_b = \mu \frac{d \ln Z_b}{d\mu}\bigg|_{FP} . \tag{3.20}$$

Note that these anomalous dimensions are gauge-dependent, and not physically observable. We have defined them in the gauge $\lambda =$ constant. In terms of the coupling constants,

$$\eta_f = g^2 + \frac{3}{4}\gamma^2 - 2g^4 - \frac{3}{4}\gamma^4 - \frac{3}{4}g^2\gamma^2\left(1 + \frac{\aleph}{2}\right) , \tag{3.21}$$

$$\eta_b = 2g^2 - 2g^4 - \frac{3}{4}g^2\gamma^2(2 - \aleph) . \tag{3.22}$$

At the fixed points, we obtain the following expressions for the anomalous dimension,

$$FP_1 : \eta_f = 0 , \quad \eta_b = 0 , \tag{3.23}$$

$$FP_2 : \eta_f = \frac{3}{8}\epsilon , \quad \eta_b = 0 \quad \eta_f \text{ does not recieve correction at two loop } , \tag{3.24}$$

$$FP_3 : \eta_f = \frac{2}{3}\bar{r} - \frac{16}{27}\bar{r}^2 , \quad \eta_b = \frac{4}{3}\bar{r} - \frac{8}{27}\bar{r}^2 , \tag{3.25}$$

$$FP_4 : \eta_f = \frac{1}{3}\epsilon + \frac{2}{9}\bar{r} - \frac{\epsilon^2}{81} - \frac{256}{729}\bar{r}^2 + \frac{32}{243}\epsilon\bar{r} , \quad \eta_b = -\frac{1}{3}\epsilon + \frac{16}{9}\bar{r} - \frac{7}{162}\epsilon^2 - \frac{896}{729}\bar{r}^2 + \frac{112}{243}\epsilon\bar{r} . \tag{3.26}$$

E. Anomalous dimensions of the electron and spin operators

We now calculate the anomalous dimensions η_c and η_S of the physical and gauge-invariant composite operators, the electron c_α and the spin $\boldsymbol{S}$ specified in (1.3), defined such that

$$\overline{R}(\tau) \sim \frac{\mathrm{sgn}(\tau)}{|\tau|^{\eta_c}} \quad , \quad \overline{Q}(\tau) \sim \frac{1}{|\tau|^{\eta_S}} \, , \tag{3.27}$$

at large τ. We will show that it is possible to determine these anomalous dimensions to *all orders* in the ϵ and $\bar{r}$ expansions, as was also the case in previous analyses [46–51].

To compute these scaling dimensions, we add source terms to the action

$$\mathcal{S}_c = \frac{1}{\beta} \sum_{i\omega_n} \left(\Lambda_S f_\alpha^\dagger \frac{\sigma^a_{\alpha\beta}}{2} f_\beta + \Lambda_c [f_\alpha^\dagger b + H.c.] \right) . \tag{3.28}$$

Within the field-theoretic RG scheme, we have

$$\Lambda_S = \frac{Z_{ff} \Lambda_{S,R}}{Z_f} \, , \qquad \Lambda_c = \frac{Z_{fb} \Lambda_{c,R}}{\sqrt{Z_f Z_b}} \, . \tag{3.29}$$

The composite operators $\hat{S} = f_\alpha^\dagger (\sigma^a_{\alpha\beta}/2) f_\beta$ and $c_\alpha^\dagger = f_\alpha^\dagger b$ are renormalized as follows:

$$\hat{S} = \sqrt{Z_S} \hat{S}_R \, , \qquad c = \sqrt{Z_c} c_R \, . \tag{3.30}$$

It turns out that the diagrams contributing to the vertex corrections to Λ_S and Λ_c are exactly those we encountered while evaluating Z_γ and Z_g respectively. Thus we have,

$$Z_S = \left(\frac{Z_f}{Z_\gamma} \right)^2 , \qquad Z_c = \frac{Z_f Z_b}{Z_g^2} \, . \tag{3.31}$$

It is these identities which enable use to compute the anomalous dimensions exactly. We evaluate the required anomalous dimensions as,

$$\eta_S = \frac{d \ln Z_S}{d \ln \mu} \, , \qquad \eta_c = \frac{d \ln Z_c}{d \ln \mu} \, . \tag{3.32}$$

We can now make an exact statement for η_S for fixed points with $\gamma \neq 0$. From Eqns. (3.32) and (3.31) we obtain,

$$\eta_S = \frac{2}{Z_f Z_\gamma} \left[\left(Z_\gamma \frac{\partial Z_f}{\partial g} - Z_f \frac{\partial Z_\gamma}{\partial g} \right) \beta(g) + \left(Z_\gamma \frac{\partial Z_f}{\partial \gamma} - Z_f \frac{\partial Z_\gamma}{\partial \gamma} \right) \beta(\gamma) \right] . \tag{3.33}$$

Substituting the above equation in Eqn. (D4), we obtain,

$$\frac{\epsilon}{2} \gamma Z_\gamma Z_f - \gamma \eta_S \frac{Z_f Z_\gamma}{2} + \beta(\gamma) Z_f Z_\gamma = 0 \, , \tag{3.34}$$

which leads to

$$\gamma\eta_S = \gamma\epsilon + 2\beta(\gamma)\,. \tag{3.35}$$

The first term on the r.h.s. of (3.35) arises from the tree-level scaling dimension, while the second term contains potential corrections higher order in ϵ. However, at the fixed point where $\gamma = \gamma^* \neq 0$, we have $\beta(\gamma^*) = 0$ and therefore,

$$\eta_S = \epsilon\,, \quad \text{to all orders in } \epsilon \text{ and } \bar{r}. \tag{3.36}$$

The same value of η_S is also obtained in the large M expansion in (C44) and (C47).

Similarly, using Eqns. (3.32) and (3.31) in combination with Eqn. (D3) we obtain the following relation:

$$g\eta_c = 2\bar{r}g + 2\beta(g)\,. \tag{3.37}$$

Thus at the fixed point, $\beta(g^*) = 0$, such that $g^* \neq 0$, we obtain

$$\eta_c = 2\bar{r}\,, \quad \text{to all orders in } \epsilon \text{ and } \bar{r}. \tag{3.38}$$

The same value of η_c is also obtained in the large M expansion in (C34) and (C36).

We can now state the main result of this subsection: at the non-trivial fixed point FP_4 ($g^* \neq 0, \gamma^* \neq 0$) we have $\eta_S = \epsilon$ and $\eta_c = 2\bar{r}$ to all orders in ϵ and $\bar{r}$.

Finally, we can impose the self-consistency condition, Eq. (2.3). This implies equating the exponents in Eq. (2.8) to the anomalous dimensions found above, *i.e.*, $\eta_S = d - 1$ and $\eta_c = r + 1$. Solving these equations requires using values of ϵ and $\bar{r}$ which are of order unity, but because Eqs. (3.36) and (3.38) are valid to all orders, we can use such values with confidence. Solving these self-consistency conditions we obtain our exact results for η_c and η_S

$$\eta_S = 1 \quad , \quad \eta_c = 1\,, \tag{3.39}$$

at the self-consistent values $\epsilon = 1$ and $\bar{r} = 1/2$. These anomalous dimensions imply the critical correlators at FP_4

$$\langle \boldsymbol{S}(\tau)\cdot\boldsymbol{S}(0)\rangle \sim \frac{1}{|\tau|} \quad , \quad \left\langle c_\alpha(\tau)c_\alpha^\dagger(0)\right\rangle \sim \frac{\mathrm{sgn}(\tau)}{|\tau|}\,, \tag{3.40}$$

as indicated in Fig. 1. We note that the fixed point FP_4 in (3.19) is stable when evaluated at $\epsilon = 1$ and $\bar{r} = 1/2$, although formally we cannot trust our expansion for the stability exponent at such large values of ϵ and $\bar{r}$.

IV. MOVING AWAY FROM THE CRITICAL POINT

The RG flow equations presented in Section III C have a fixed point FP_4 which realizes the deconfined critical point of Fig. 1. This fixed point has one relevant direction, corresponding to

the on-site energy s which distinguishes the local energy of the spinon and holon states. As s flows to $+\infty$, the holon state is lower in energy, corresponding to the $p > p_c$ region of the phase diagram in Fig. 1. Conversely, as s flows to $-\infty$, the spinon states are lower in energy, corresponding to the $p < p_c$ region of the phase diagram.

We can now exploit the choice of superspin representations between SU(1|2) and SU(2|1) to understand the fate of the RG flow. The energy of the ground state is minimized if we maximize the occupation of the lower energy state, and this is achieved if we choose the representation in which this lower energy state is bosonic. This implies that we should choose SU(1|2) for $p > p_c$ and SU(2|1) for $p < p_c$, as indicated in Fig. 1. We now describe the structure of these theories in turn

A. Overdoped region

In the SU(1|2) theory for $p > p_c$, we condense the boson b. With $\langle b \rangle \neq 0$, we have from (1.3), $c_\alpha \sim f_\alpha$, and the hopping term t_{ij} in H_{tJ} in (1.1) reduces to a renormalized hopping term for the f_α spinons. Indeed, the resulting theory for the f_α fermions is similar to that studied by Parcollet and Georges [24], and more recently in SYK-like extensions [62–66].

A description of this phase, far from the $p = p_c$ critical point, can be obtained from H_{tJ} in (1.1) by taking the large M limit of Ref. 24: we consider spinons f_α with $\alpha = 1 \ldots M$, the bosons b do not acquire any additional index (so we are considering a SU(1|M) superspin), and we rescale $t^2 \to t^2/M^2$ and $J^2 \to J^2/M$. (Note that this large M limit is distinct from that described in our Appendix C, where the bosons do acquire an additional index, and we rescale $t^2 \to t^2/M$ and $J^2 \to J^2/M$.)

In the large M limit of Ref. 24, the b bosons can be replaced by their condensate $\langle b \rangle = b_0\sqrt{M}$. The f_α fermions have an effective hopping of strength $t\, b_0^2$. As shown in Ref. 24, the theory behaves a like a disordered Fermi liquid below a coherence scale

$$E_c = \frac{(t b_0^2)^2}{J}. \tag{4.1}$$

Note that this disordered Fermi liquid has a hole carrier density of $1+p$. This follows from $c_\alpha \sim f_\alpha$, and the density of f_α fermions obtained from (1.4) and (2.5).

As we approach the critical point, with $p \searrow p_c$, we expect E_c and $\langle b \rangle$ to both vanish algebraically. However, we do not expect the large M theory of Ref. 24 to properly describe the approach to the critical point: in this large M theory, we obtain an insulating state as $\langle b \rangle$ vanishes, whereas our $p = p_c$ critical point is metallic. Indeed, as b is gauge-charged field, the value of $\langle b \rangle$ is not a gauge-invariant quantity which can be directly compared between different approaches. However, the crossover scale E_c is better defined, and we can deduce the behavior of E_c near $p = p_c$ by the

RG analysis of Section III. We expect

$$E_c \sim |p - p_c|^{1/\lambda_s} \tag{4.2}$$

where λ_s is the relevant RG eigenvalue with which s flows away from the FP_4 fixed point, specified in (D13).

B. Pseudogap region

For $p < p_c$, we use the SU(2|1) theory, and condense the $\mathfrak{b}_\alpha$ spinons to obtain spin glass order, as described in Refs. [27, 28]. The presence of the mobile $\mathfrak{f}$ fermions will make this a metallic spin glass with carrier density p, as determined by (2.7).

We need to extend the insulating spin glass theory of Refs. [27, 28] to the metallic spin glass, and this will be studied in greater detail in future work. Here we note that a systematic description appears possible in the large M limit of a SU($M|M'$) formulation noted in Appendix A 1, where the $\mathfrak{f}$ fermions acquire an additional 'orbital' label $\ell = 1 \ldots M'$, and we keep $k = M'/M$ fixed in the large M limit. This should be contrasted from the SU($M'|M$) theory described in Appendix C, in which the b_ℓ bosons are assumed to not condense.

C. Specific heat

This section discusses qualitative features of the specific across the phase transition at $p = p_c$.

Right at $p = p_c$, the critical theory is expected [28] to have a non-vanishing extensive entropy S_0 as $T \to 0$. This follows from the similarity of the random insulating magnet [18], and many other models in the SYK class.

Away from $p = p_c$, we expect that the entropy follows the behavior of the critical point at temperatures above the coherence scale E_c, before vanishing lineary with T at temperatures below E_c, as shown in Fig. 4. We can therefore estimate that the linear-in-T coefficient of the specific heat C is

$$\gamma = \lim_{T\to 0} \frac{C}{T} = \lim_{T\to 0} \frac{dS}{dT} \sim \frac{S_0}{E_c} \tag{4.3}$$

So we expect γ to diverge as $|p - p_c|^{-1/\lambda_s}$ in the infinite range model H_{tJ}. It is notable that this behavior resembles experimental observations [8].

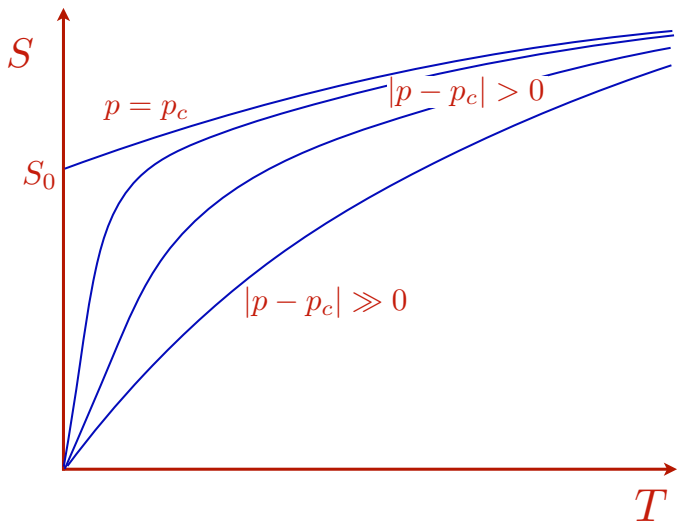

FIG. 4. Schematic plot of the temperature dependence of the entropy S of H_{tJ}. At $p = p_c$, there is a non-vanishing extensive entropy at zero temperature S_0. The linear-in-T coefficient of the specific heat $\gamma = \lim_{T\to 0} C/T = \lim_{T\to 0} dS/dT$ diverges as we approach p_c.

V. CONCLUSIONS

We have presented a RG analysis (in Section III) of the phase diagram of the t-J model in (1.1) with random and all-to-all hopping and spin exchange. The predictions of this analysis are presented in Fig. 1: a deconfined critical point which separates two phases without fractionalization: a 'pseudogap' metallic spin glass phase with carrier density p, from a disordered Fermi liquid with carrier density $1 + p$. The change in the carrier density across the critical point, and the behavior of the specific heat across the critical point implied by the entropy in Fig. 4 are in good qualitative accord with experimental observations [5–8]. The SYK-like structure of the deconfined critical point connects naturally with a class of theories with linear-in-T resistivity in the strange metal [24, 62–66]; a linear-in-T resistivity was also found in numerical studies [40, 41] of lattice models without disorder described by equations closely related to those of the large M limit of Appendix C. And we note that there is a recent report of spin glass correlations in the pseudogap phase [13], extending earlier impurity-induced observations [11, 12].

It is useful to compare the structure of H_{tJ} in (1.1) with that of SYK lattice models [62–65]. The SYK models have a random 4-fermion interaction term, and a random 2-fermion hopping term of strength t, but no on-site fermion constraint. At the lowest energies, the 2-fermion term is always relevant and drives the system away from SYK criticality to a Fermi liquid state. In the present t-J model analysis, the presence of the local constraint (1.4) or (1.6) is crucial; in

terms of the fractionalized particles in (1.3) or (1.5), *both* the t and J terms are 4-particle terms. Consequently, they can balance each other, and allow for a critical SYK-like state to exist at a critical $p = p_c$ all the way down to $T = 0$. At $p = p_c$, the 3 states of the t-J model obeying the constraint (1.4) or (1.6) are nearly degenerate in our perturbative renormalization group analysis. Consequently, we find $p_c = 1/3$ at zeroth order (see Fig. 1).

Appendix C presents a low energy analysis of the large M saddle point of H_{tJ} obtained by generalizing the SU(2) symmetry to SU(M). The main difference from the RG analysis is that a critical *phase* appears in the low energy and large M theory, rather than a critical point. However, the exponents of the gauge-invariant spin and electron operators in the appropriate large M phase are the *same* as those obtained by the renormalization group analysis of the deconfined critical point to all orders in ϵ and $\bar{r}$: compare (C44,C47) and (C34,C36) with (3.36) and (3.38). We also note that the similarity between Appendix C and the SYK equations indicates that our critical theory obeys maximal chaos [17].

A useful perspective on our renormalization group analysis provided by viewing the 3 states on each site as different orientations of a SU(1|2) or SU(2|1) superspin [32]. In the large N limit of a N-site t-J model with random and all-to-all interactions, we obtain an impurity model in which the superspin is coupled to both fermionic and bosonic baths self-consistently. In addition, there is a 'Zeeman field' acting on the superspin which breaks the degeneracy between the spinon and holon states; this field is a strongly relevant perturbation at the deconfined critical point, and drives the system into the two phases flanking the critical point. (See Refs. [59–61] for analogous RG studies of a relevant "Zeeman field" at an impurity site (represented by a SU(2) spin) in a Bose-Hubbard model at the superfluid-insulator transition, which are in good agreement with numerics.) In the overdoped phase, the holon state has a lower energy (see Fig. 1): so we use the SU(1|2) superspin in which the holon is a boson, and condense it to obtain a disordered Fermi liquid, analogously to Ref. 24. Conversely, in the underdoped phase, the spinon states have a lower energy, so we use the SU(2|1) superspin in which the spinons are bosons, and condense them to obtain a metallic spin glass.

Despite our use of the superspin terminology, the model studied and the renormalization group equations are not supersymmetric: the fermionic c_α generators in (1.3) and (1.5) do not commute with the Hamiltonian. We can extend H_{tJ} by including off-site interations with the generator V in (1.3) and (1.5), and this will include density-density interactions. With this extension, we have the possibility of charge glass order in the pseudogap, and critical density fluctuations (likely similar to those observed in Refs. 67 and 68) at possibly supersymmetric fixed points. (Supersymmetric t-J models have been studied in one dimension without disorder [69–73].)

Finally, we comment on the extent to which a model with all-to-all randomness can be mapped to the cuprates. Randomness is present in the experimental systems, and also serves important

simplifying purposes in our theoretical analysis. Moreover, certain approximations to models without randomness lead to closely related saddle point equations [23, 39–41]. Several of the broken symmetries do not exist in the random model, and subtle questions [74] about the structure of the Fermi surface in momentum space can be avoided. However, the central issues of carrier density, fractionalization, emergent gauge charges, and associated quantum phase transitions remain well defined even in the presence of randomness. Given the recent spin glass observations [13], and as we noted in Section IV B, it will be useful to study the metallic pseudogap state, and the interplay between the spin glass order and charge transport. A possible approach is the extend the large M theory of Refs. [27, 28] to include fermionic holons, as well as numerical studies for $M = 2$.

Acknowledgements

We thank P. Cha, J.C. Seamus Davis, M.-H. Julien, E.-A. Kim, G. Kotliar, O. Parcollet, N. Seiberg, A. Sengupta, Z.-X. Shen, Qimiao Si, T. Senthil, L. Taillefer, M. Vojta, and Ya-Hui Zhang for valuable discussions. This research was supported by the National Science Foundation under Grant No. DMR-1664842 and U.S. Department of Energy under Grant DE-SC0019030. G.T. acknowledges support from the MURI grant W911NF-14-1-0003 from ARO and by DOE grant DE-SC0007870. The Flatiron Institute is a division of the Simons Foundation.

Appendix A: Superalgebras

The operators in (1.3) obey the commutation and anti-commutation relations

$$\begin{aligned} [S^a, S^b] = i\epsilon_{abc} S^c \quad , \quad \{c_\alpha, c_\beta\} = 0 \quad , \quad \{c_\alpha, c_\beta^\dagger\} = \delta_{\alpha\beta} V + \sigma^a_{\alpha\beta} S^a \\ [S^a, c_\alpha] = -\frac{1}{2}\sigma^a_{\alpha\beta} c_\beta \quad , \quad [S^a, c_\alpha^\dagger] = \frac{1}{2}\sigma^a_{\beta\alpha} c_\beta^\dagger \quad , \quad [S^a, V] = 0 \\ [V, c_\alpha] = \frac{1}{2} c_\alpha \quad , \quad [V, c_\alpha^\dagger] = -\frac{1}{2} c_\alpha^\dagger \, . \end{aligned} \tag{A1}$$

The constraint (1.4) commutes with all operators of the superalgebra. Imposing this constraint yields the fundamental representation of SU(1|2).

Alternatively, we can use the operators in (1.5). These realize the SU(2|1) algebra, and it can be verified that these operators also obeys the superalgebra in Eq. (A1). The constraint projecting to the fundamental representation is now (1.6).

1. Larger symmetries

We consider the model for general M and M', with the electron operator

$$c_{\ell\alpha} = b^\dagger_\ell f_\alpha \,, \tag{A2}$$

acquiring both spin ($\alpha = 1 \ldots M$) and 'orbital' ($\ell = 1 \ldots M'$) indices. We define the SU(M) spin operator

$$S^a = f^\dagger_\alpha T^a_{\alpha\beta} f_\beta \tag{A3}$$

where the matrices T^a obey

$$\mathrm{tr}(T^a T^b) = \frac{1}{2}\delta^{ab}, \quad T^a T^a = \frac{M^2-1}{2M}\cdot \mathbf{1}\,, \quad T^a_{\alpha\beta} T^a_{\gamma\delta} = \frac{1}{2}\Big(\delta_{\alpha\delta}\delta_{\beta\gamma} - \frac{1}{M}\delta_{\alpha\beta}\delta_{\gamma\delta}\Big)\,. \tag{A4}$$

The operators $c_{\ell\alpha}$, S^a, the operator

$$V = \frac{1}{M} f^\dagger_\alpha f_\alpha + \frac{1}{M'} b^\dagger_\ell b_\ell \,, \tag{A5}$$

and the operators $b^\dagger_\ell T^a_{\ell\ell'} b_{\ell'}$ are the $(M+M')^2 - 1$ generators of the superalgebra SU($M'|M$).

A general constraint fixing the representation is

$$f^\dagger_\alpha f_\alpha + b^\dagger_\ell b_\ell = P \,, \tag{A6}$$

with P a positive integer, and our interest in the case $P = M/2$ which realizes the representation in which the SU(M) subalgebra is self-conjugate. Note that the fundamental representation of the superalgebra is $P = 1$, but this does not lead to a convenient large M limit.

We can also consider a bosonic spinon and fermionic holon decomposition for general M, M'

$$c_{\ell\alpha} = \mathfrak{f}^\dagger_\ell \mathfrak{b}_\alpha \tag{A7}$$

The analogous steps will lead to a realization of the SU($M|M'$) superalgebra, which is identical to the SU($M'|M$) superalgebra. However, the constraint

$$\mathfrak{b}^\dagger_\alpha \mathfrak{b}_\alpha + \mathfrak{f}^\dagger_\ell \mathfrak{f}_\ell = P \tag{A8}$$

now leads to a *different representation* of the superalgebra from (A6) for $P \neq 1$ [75]. So the models defined by (A2) and (A7) are in general different, although they are the same for the $M = 2$, $M' = 1$ case of interest to us. Note also that in all cases the Hamiltonian contains an exchange interaction involving the SU(M) generators only, and not the SU(M') generators.

2. Operator expectation values

We will compute the only RG equations for the SU($M'|M$) theory in Appendix B following the method in Appendix C of Ref. 47. After using the identity (A4), the computations in Appendix B can be reduced to the following operator traces.

First, let us compute the dimension, $\mathcal{D}(M, M', P)$, of the superspin Hilbert space. To compute this, it is useful to compute the grand-canonical partition function, while ignoring the constraint (A6).

$$\mathcal{Z}(z) = \mathrm{Tr}\, z^{f_\alpha^\dagger f_\alpha + b_\ell^\dagger b_\ell} = \frac{(1+z)^M}{(1-z)^{M'}} \tag{A9}$$

where z is the common fugacity. Then we can impose the constraint (A6), and the dimension of the Hilbert space is given by the coefficient of z^P in the series expansion of $\mathcal{Z}(z)$, or equivalently

$$\mathcal{D}(M, M', P) = \oint_{|z|=c<1} \frac{dz}{2\pi i} \frac{1}{z^{P+1}} \mathcal{Z}(z) \tag{A10}$$

Some sample values from Mathematica are

$$\mathcal{D}(2,1,1) = 3 \quad , \quad \mathcal{D}(6,6,3) = 292 \quad , \quad \mathcal{D}(20,14,10) = 553844224 \quad , \quad \ldots \tag{A11}$$

Now we can compute the general expectation value

$$\begin{aligned} \mathcal{I}_{m,m'} &\equiv \left\langle \left(f_\alpha^\dagger f_\alpha\right)^m \left(b_\ell^\dagger b_\ell\right)^{m'} \right\rangle \\ &= \frac{1}{\mathcal{D}(M, M', P)} \oint_{|z|=c<1} \frac{dz}{2\pi i} \frac{1}{z^{P+1}} \left[\left(z\frac{d}{dz}\right)^m (1+z)^M\right] \left[\left(z\frac{d}{dz}\right)^{m'} \frac{1}{(1-z)^{M'}}\right] . \end{aligned} \tag{A12}$$

Note $\mathcal{I}_{0,0} = 1$.

The values for $M = 2$, $P = 1$, and $M' = 1$ case of interest to us are simple:

$$\mathcal{I}_{m,0} = \frac{2}{3}, \quad m \geq 1; \quad \mathcal{I}_{0,m'} = \frac{1}{3}, \quad m' \geq 1; \quad \mathcal{I}_{m,m'} = 0, \quad m \geq 1 \text{ and } m' \geq 1\,. \tag{A13}$$

This simplicity is the reason Section III was able to compute the RG equations using Feynman diagrams and the Abrikosov method.

Some other random values

$$\begin{aligned} \mathcal{I}_{2,3} = \frac{342}{73}, \quad \mathcal{I}_{7,4} = \frac{3384}{73}, \quad &\text{for } M = 6,\ M' = 6,\ P = 3; \\ \mathcal{I}_{7,4} = \frac{238531161015}{6698}, \quad \mathcal{I}_{3,9} = \frac{3197447102115}{6698}, \quad &\text{for } M = 20,\ M' = 14,\ P = 10. \end{aligned} \tag{A14}$$

Appendix B: RG equations for general M, M'

This appendix generalizes the method of Refs. [46, 47] for SU(2) spins to superspins in SU($M'|M$). This method utilizes only gauge-invariant information contained in the superspin algebra and its representation; thus the Berry phase $\mathcal{S}_B$ (see (2.4) and (2.6)) of the supergroup [32] is exactly accounted for by the commutation and anti-commutation relations. The RG equations obtained here reduce to those of Section III at $M = 2$, $P = 1$, $M' = 1$.

We consider here the Hamiltonian

$$H_{\rm imp} = g_0 \left(c^\dagger_{\ell\alpha}\, \psi_{\alpha\ell}(0) + \text{H.c.} \right) + \gamma_0 S^a\, \phi_a(0) + \int |k|^r dk\, k\, \psi^\dagger_{k\alpha\ell} \psi_{k\alpha\ell} + \frac{1}{2} \int d^d x \left[\pi_a^2 + (\partial_x \phi_a)^2 \right] , \tag{B1}$$

where $c_{\ell\alpha}$ and S^a are defined in (A2) and (A3), and we impose exactly the constraint (A6). Recall, the indices $\alpha, \beta = 1 \ldots M$, $\ell = 1 \ldots M'$, and $a = 1 \ldots M^2 - 1$.

The setup of the renormalization factors in the present perturbation theory is somewhat different from (3.2). We now write, using the operators defined in (A2) and (A3),

$$S^a = \sqrt{Z_S} S^a_R\,, \quad c_{\ell\alpha} = \sqrt{Z_c} c_{R,\ell\alpha}\,, \quad \gamma_0 = \frac{\mu^{\epsilon/2} \widetilde{Z}_\gamma}{\sqrt{Z_S \widetilde{S}_{d+1}}} \gamma\,, \quad g_0 = \frac{\mu^{\bar{r}} \widetilde{Z}_g}{\sqrt{Z_c \Gamma(r+1)}} g\,. \tag{B2}$$

The renormalization constants Z_S and Z_c are the same as those defined in (3.30), but we will now compute them in a different manner. The notation of our renormalization constants also differs from that in Ref. 48, and we provide a translation in Table I. Unlike Ref. 48, we do not have bulk

Ref. 48	Present paper
Z_h	Z_f
$\widetilde{Z}_\gamma$	Z_γ
Z	$Z_\phi = 1$
Z'	Z_S
Z_γ	$\widetilde{Z}_\gamma = 1$

TABLE I. Correspondence between the notations of Ref. 48 and the present paper.

interactions of the bosonic bath field ϕ, and hence we have $Z_\phi = 1$, as we noted in Section III C. For the same reasons, it was argued in Refs. [46–48] that (in our notation) $\widetilde{Z}_\gamma = 1$ in the absence of bulk interactions. The reasoning extends also to the fermionic bath, and so we have $\widetilde{Z}_\gamma = 1$ and $\widetilde{Z}_g = 1$ exactly. These identities can also be understood from the statement below (3.30) that the vertex corrections $\Lambda_{S,c}$ arise from the same diagrams as $Z_{\gamma,g}$. We will now compute Z_S and Z_c by renormalizing the two-point correlators of S^a and $c_{\ell\alpha}$, and this will sufficient to obtain the needed beta functions.

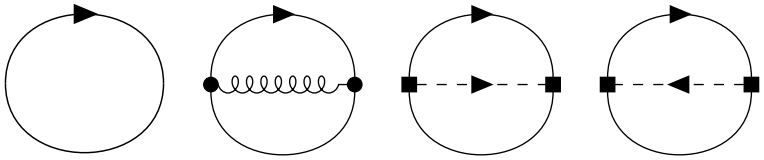

(a) (b) (c) (d)

FIG. 5. Diagrams contributing to the denominator, D (Eq. (B3)), of $\langle O_1 \rangle = \langle S^a(\tau) S^a(0) \rangle$. The oriented line denotes the trajectory of the SU($M'|M$) superspin in imaginary time, a filled circle is a γ_0 vertex, and a filled square is a g_0 vertex. The spiral curve denotes the ϕ propagator, and the dashed curve represents the ψ propagator.

1. Spin correlator

This subsection evaluates the spin correlator, $\langle O_1 \rangle \equiv \langle S^a(\tau) S^a(0) \rangle$, and its renormalization will yield Z_S. We follow the strategy of Ref. 47: use time-ordered perturbation theory to expand the correlator in powers of g_0 and γ_0, insert the two-point correlators of the bulk fields, and then explicitly evaluate the traces over the S^a and $c_{\ell\alpha}$ operators using the superspin algebra described in Appendix A. This effectively exactly evaluates the path integral over the Berry phase $\mathcal{S}_B$ in (2.4).

We write the correlator as $\langle O_1 \rangle = N_1/D$, and the perturbative expansions of the numerator and denominator are represented by the diagrams shown in Figs. 5 and 6. Note that these are not Feynman diagrams, and there is no Wick's theorem. The oriented line represents the worldline of the superspin, and the diagrams indicate the ordering of the operators whose traces are to be evaluated. The numerator and denominator have to be evaluated separately, and there is no automatic cancellation of disconnected contributions. The diagrams in Figs. 5 and 6 yield

$$\begin{aligned} D = 1 &+ \gamma_0^2 L_0 \left(D_{1\phi} + D_{2\phi} + D_{3\phi} \right) + g_0^2 L_0' \left(D_{1\psi}' + D_{2\psi}' + D_{3\psi}' \right) \\ &+ g_0^2 L_0'' \left(D_{1\psi}'' + D_{2\psi}'' + D_{3\psi}'' \right) , \end{aligned} \tag{B3}$$

$$\begin{aligned} N_1 = L_0 &+ \gamma_0^2 \left(L_1 D_{1\phi} + L_2 D_{2\phi} + L_3 D_{3\phi} \right) + g_0^2 \left(L_1' D_{1\psi}' + L_2' D_{2\psi}' + L_3' D_{3\psi}' \right) \\ &+ g_0^2 \left(L_1'' D_{1\psi}'' + L_2'' D_{2\psi}'' + L_3'' D_{3\psi}'' \right) , \end{aligned} \tag{B4}$$

where the average over the supergroup representation $\langle \mathcal{O} \rangle \equiv (\mathrm{Tr}\mathcal{O}) / (\mathrm{Tr}\mathbb{1})$, $\mathrm{Tr}\mathbb{1} = \mathcal{D}(M, M', P)$, is carried out by the expressions

$$L_0 = \langle S^a S^a \rangle = \frac{M+1}{2M} (M\mathcal{I}_{1,0} - \mathcal{I}_{2,0}) , \tag{B5}$$

$$L_0' = \left\langle c_{\ell\alpha} c_{\ell\alpha}^\dagger \right\rangle = -\mathcal{I}_{1,1} + M\mathcal{I}_{0,1} , \tag{B6}$$

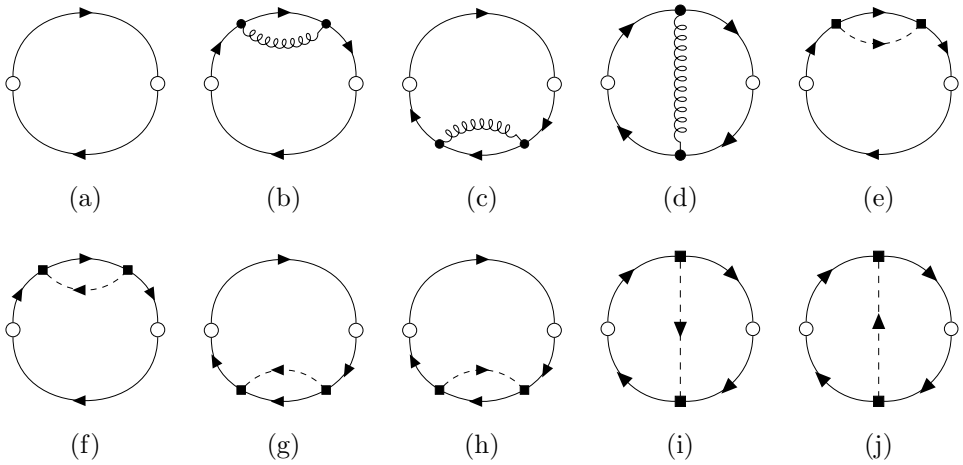

FIG. 6. Diagrams contributing to the numerator, N_1 (Eq. (B4)), of $\langle O_1\rangle = \langle S^a(\tau)S^a(0)\rangle$. Conventions as in Fig. 5, and an open circle denotes the external S^a operator.

$$L_0'' = \left\langle c_{\ell\alpha}^\dagger c_{\ell\alpha}\right\rangle = M'\mathcal{I}_{1,0} + \mathcal{I}_{1,1}\,, \tag{B7}$$

$$L_1 = \left\langle S^a S^b S^b S^a\right\rangle = \frac{(M+1)^2}{4M^2}(M^2\mathcal{I}_{2,0} + \mathcal{I}_{4,0} - 2M\mathcal{I}_{3,0})\,, \tag{B8}$$

$$L_2 = \left\langle S^a S^a S^b S^b\right\rangle = \frac{(M+1)^2}{4M^2}(M^2\mathcal{I}_{2,0} + \mathcal{I}_{4,0} - 2M\mathcal{I}_{3,0})\,, \tag{B9}$$

$$L_3 = \left\langle S^a S^b S^a S^b\right\rangle = \frac{M+1}{4M^2}(-M^3\mathcal{I}_{1,0} + M^2(M+2)\mathcal{I}_{2,0} - 2M(M+1)\mathcal{I}_{3,0} + (M+1)\mathcal{I}_{4,0})\,, \tag{B10}$$

$$L_1' = \left\langle S^a c_{\ell\alpha} c_{\ell\alpha}^\dagger S^a\right\rangle = -\frac{M+1}{2M}(2M\mathcal{I}_{2,1} - M^2\mathcal{I}_{1,1} - \mathcal{I}_{3,1})\,, \tag{B11}$$

$$L_2' = \left\langle S^a S^a c_{\ell\alpha} c_{\ell\alpha}^\dagger\right\rangle = -\frac{M+1}{2M}(2M\mathcal{I}_{2,1} - M^2\mathcal{I}_{1,1} - \mathcal{I}_{3,1})\,, \tag{B12}$$

$$L_3' = \left\langle S^a c_{\ell\alpha} S^a c_{\ell\alpha}^\dagger\right\rangle = -\frac{M+1}{2M}((2M-1)\mathcal{I}_{2,1} - M(M-1)^2\mathcal{I}_{1,1} - \mathcal{I}_{3,1})\,, \tag{B13}$$

$$L_1'' = \left\langle S^a c_{\ell\alpha}^\dagger c_{\ell\alpha} S^a\right\rangle = \frac{M+1}{2M}(MM'\mathcal{I}_{2,0} - M'\mathcal{I}_{3,0} + M\mathcal{I}_{2,1} - \mathcal{I}_{3,1})\,, \tag{B14}$$

$$L_2'' = \left\langle S^a S^a c_{\ell\alpha}^\dagger c_{\ell\alpha}\right\rangle = \frac{M+1}{2M}(MM'\mathcal{I}_{2,0} - M'\mathcal{I}_{3,0} + M\mathcal{I}_{2,1} - \mathcal{I}_{3,1})\,, \tag{B15}$$

$$L_3'' = \left\langle S^a c_{\ell\alpha}^\dagger S^a c_{\ell\alpha}\right\rangle = \frac{M+1}{2M}(M'(M+1)\mathcal{I}_{2,0} - MM'\mathcal{I}_{1,0} - M'\mathcal{I}_{3,0} + (M+1)\mathcal{I}_{2,1} - M\mathcal{I}_{1,1} - \mathcal{I}_{3,1})\,. \tag{B16}$$

Also,

$$`D_{1\phi} = \int_0^\tau d\tau_1 \int_{\tau_1}^\tau d\tau_2 G_\phi(\tau_1-\tau_2) = -\frac{\widetilde{S}_{d+1}\tau^\epsilon}{\epsilon(1-\epsilon)}\,, \tag{B17}$$

$$D_{2\phi} = \int_{\tau}^{\beta} d\tau_1 \int_{\tau_1}^{\beta} d\tau_2 G_\phi(\tau_1 - \tau_2) = -\frac{\widetilde{S}_{d+1}\tau^\epsilon}{\epsilon(1-\epsilon)}\,, \tag{B18}$$

$$D_{3\phi} = \int_{0}^{\tau} d\tau_1 \int_{\tau}^{\beta} d\tau_2 G_\phi(\tau_1 - \tau_2) = \frac{2\widetilde{S}_{d+1}\tau^\epsilon}{\epsilon(1-\epsilon)}\,, \tag{B19}$$

$$D'_{1\psi} = \int_{0}^{\tau} d\tau_1 \int_{\tau_1}^{\tau} d\tau_2 G_\psi(\tau_2 - \tau_1) = -\frac{\Gamma(r+1)\tau^{2\bar{r}}}{2\bar{r}(1-2\bar{r})}\,, \tag{B20}$$

$$D'_{2\psi} = \int_{\tau}^{\beta} d\tau_1 \int_{\tau_1}^{\beta} d\tau_2 G_\psi(\tau_2 - \tau_1) = -\frac{\Gamma(r+1)\tau^{2\bar{r}}}{2\bar{r}(1-2\bar{r})}\,, \tag{B21}$$

$$D'_{3\psi} = \int_{0}^{\tau} d\tau_1 \int_{\tau}^{\beta} d\tau_2 G_\psi(\tau_2 - \tau_1) = \frac{2\Gamma(r+1)\tau^{2\bar{r}}}{2\bar{r}(1-2\bar{r})}\,, \tag{B22}$$

$$D''_{1\psi} = -\int_{0}^{\tau} d\tau_1 \int_{\tau_1}^{\tau} d\tau_2 G_\psi(\tau_1 - \tau_2) = -\frac{\Gamma(r+1)\tau^{2\bar{r}}}{2\bar{r}(1-2\bar{r})}\,, \tag{B23}$$

$$D''_{2\psi} = -\int_{\tau}^{\beta} d\tau_1 \int_{\tau_1}^{\beta} d\tau_2 G_\psi(\tau_1 - \tau_2) = -\frac{\Gamma(r+1)\tau^{2\bar{r}}}{2\bar{r}(1-2\bar{r})}\,, \tag{B24}$$

$$D''_{3\psi} = -\int_{0}^{\tau} d\tau_1 \int_{\tau}^{\beta} d\tau_2 G_\psi(\tau_1 - \tau_2) = -\frac{2\Gamma(r+1)\tau^{2\bar{r}}}{2\bar{r}(1-2\bar{r})}\,. \tag{B25}$$

Note we evaluate the above integrals at $T = 0$, by extending the integrals appropriately as explained in Ref. 47. Here,

$$G_\phi(\tau) = \int \frac{d^d k}{(2\pi)^d}\frac{d\omega}{2\pi}\frac{e^{-i\omega\tau}}{k^2+\omega^2} = \frac{\widetilde{S}_{d+1}}{|\tau|^{d-1}}\,. \tag{B26}$$

Similarly,

$$\begin{aligned} G_\psi(\tau) &= \int dk|k|^r \int \frac{d\omega}{2\pi}\frac{e^{-i\omega\tau}}{i\omega - k} \\ &= \int dk|k|^r \left[-e^{-k\tau}\left(\theta(k)\theta(\tau) - \theta(-k)\theta(-\tau)\right)\right] \\ &= \frac{\Gamma(1+r)}{|\tau|^{1+r}}\left[\theta(-\tau) - \theta(\tau)\right]\,. \end{aligned} \tag{B27}$$

From (B3) and (B4) we obtain,

$$\begin{aligned} \langle O_1\rangle = \frac{N_1}{D} = \frac{L_0}{M}\Bigg\{1 &+ \gamma_0^2\left[\left(\frac{L_1}{L_0} - \frac{L_0}{M}\right)D_{1\phi} + \left(\frac{L_2}{L_0} - \frac{L_0}{M}\right)D_{2\phi} + \left(\frac{L_3}{L_0} - \frac{L_0}{M}\right)D_{3\phi}\right] \\ &+ g_0^2\left[\left(\frac{L'_1}{L_0} - \frac{L'_0}{M}\right)D'_{1\psi} + \left(\frac{L'_2}{L_0} - \frac{L'_0}{M}\right)D'_{2\psi} + \left(\frac{L'_3}{L_0} - \frac{L'_0}{M}\right)D'_{3\psi}\right] \\ &+ g_0^2\left[\left(\frac{L''_1}{L_0} - \frac{L''_0}{M}\right)D''_{1\psi} + \left(\frac{L''_2}{L_0} - \frac{L''_0}{M}\right)D''_{2\psi} + \left(\frac{L''_3}{L_0} - \frac{L''_0}{M}\right)D''_{3\psi}\right]\Bigg\}\,. \end{aligned} \tag{B28}$$

It is then straightforward to write,

$$Z_S = 1 - \frac{\gamma^2}{\epsilon}L_\gamma - \frac{g^2}{2\bar{r}}L_g\,, \tag{B29}$$

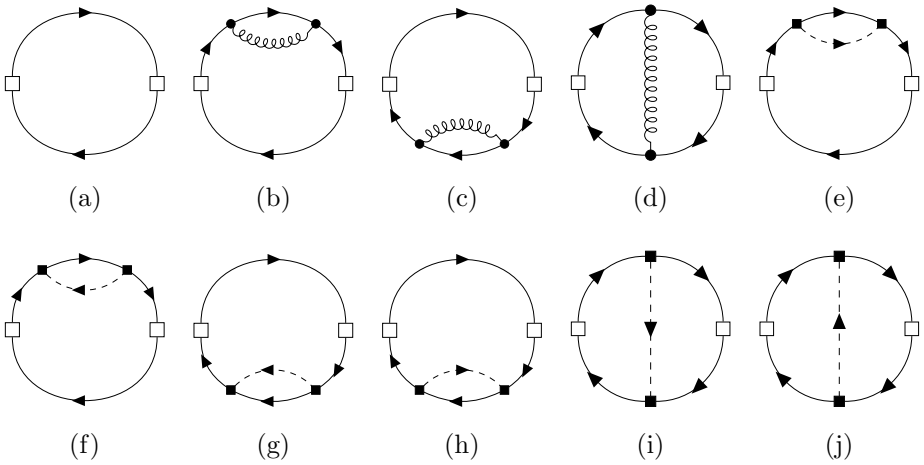

FIG. 7. Diagrams contributing to the numerator, N_2 (Eq. (B32)), of $\langle O_2\rangle = \langle c(\tau)c^\dagger(0)\rangle$. Here conventionas are as in Fig. 5, and open square denotes the external $c/c^\dagger$ operator.

where ,

$$L_\gamma = \frac{L_1 + L_2 - 2L_3}{L_0}\,, \tag{B30}$$

$$L_g = \frac{L_1' + L_1'' + L_2' + L_2'' - 2L_3' - 2L_3''}{L_0}\,. \tag{B31}$$

Note that for $M = 2\,, M' = 1$, we obtain $L_\gamma = L_g = 2$ which agrees with the result that can be obtained from (3.31) and the results in Section III.

2. Electron correlator

Next we evaluate the electron correlation, $\langle O_2\rangle \equiv \langle c(\tau)c^\dagger(0)\rangle = N_2/D$. The diagrams contributing to the numerator are shown in Fig. 7, while those contributing to the denominator have been already evaluated in (B3). Thus we obtain,

$$\begin{aligned} N_2 = P_0 &+ \gamma_0^2\left(P_1 D_{1\phi} + P_2 D_{2\phi} + P_3 D_{3\phi}\right) + g_0^2\left(P_1' D_{1\psi}' + P_2' D_{2\psi}' + P_3' D_{3\psi}'\right) \\ &+ g_0^2\left(P_1'' D_{1\psi}'' + P_2'' D_{2\psi}'' + P_3'' D_{3\psi}''\right)\,, \end{aligned} \tag{B32}$$

where,

$$P_0 = \left\langle c_{\ell\alpha}^\dagger c_{\ell\alpha}\right\rangle = M'\mathcal{I}_{1,0} + \mathcal{I}_{1,1}\,, \tag{B33}$$

$$\begin{aligned} P_1 = \left\langle c_{\ell\alpha}^\dagger S^a S^a c_{\ell\alpha}\right\rangle = \frac{M+1}{2M}&(M'(M+2)\mathcal{I}_{2,0} - M'(M+1)\mathcal{I}_{1,0} - M'\mathcal{I}_{3,0} + (M+2)\mathcal{I}_{2,1} \\ &- (M+1)\mathcal{I}_{1,1} - \mathcal{I}_{3,1})\,, \end{aligned} \tag{B34}$$

$$P_2 = \left\langle c^\dagger_{\ell\alpha} c_{\ell\alpha} S^a S^a \right\rangle = \frac{M+1}{2M}(MM'\mathcal{I}_{2,0} - M'\mathcal{I}_{3,0} + M\mathcal{I}_{2,1} - \mathcal{I}_{3,1})\,, \tag{B35}$$

$$P_3 = \left\langle c^\dagger_{\ell\alpha} S^a c_{\ell\alpha} S^a \right\rangle = \frac{M+1}{2M}(M'(M+1)\mathcal{I}_{2,0} - MM'\mathcal{I}_{1,0} - M'\mathcal{I}_{3,0} + (M+1)\mathcal{I}_{2,1} - M\mathcal{I}_{1,1} - \mathcal{I}_{3,1})\,, \tag{B36}$$

$$P'_1 = \left\langle c^\dagger_{\ell\alpha} c_{\ell'\beta} c^\dagger_{\ell'\beta} c_{\ell\alpha} \right\rangle = (M+1)M'\mathcal{I}_{1,0} - M'\mathcal{I}_{2,0} + (M+1)(M'+1)\mathcal{I}_{1,1} + (M+1)\mathcal{I}_{1,2} - (M'+1)\mathcal{I}_{2,1} - \mathcal{I}_{2,2}\,, \tag{B37}$$

$$P'_2 = \left\langle c^\dagger_{\ell\alpha} c_{\ell\alpha} c_{\ell'\beta} c^\dagger_{\ell'\beta} \right\rangle = MM'\mathcal{I}_{1,1} + M\mathcal{I}_{1,2} - M'\mathcal{I}_{2,1} - \mathcal{I}_{2,2}\,, \tag{B38}$$

$$P'_3 = \left\langle c^\dagger_{\ell\alpha} c_{\ell'\beta} c_{\ell\alpha} c^\dagger_{\ell'\beta} \right\rangle = -MM'\mathcal{I}_{1,1} - M\mathcal{I}_{1,2} + M'\mathcal{I}_{2,1} + \mathcal{I}_{2,2}\,, \tag{B39}$$

$$P''_1 = \left\langle c^\dagger_{\ell\alpha} c^\dagger_{\ell'\beta} c_{\ell'\beta} c_{\ell\alpha} \right\rangle = M'(M'+1)(\mathcal{I}_{2,0} - \mathcal{I}_{1,0}) + (2M'+1)(\mathcal{I}_{2,1} - \mathcal{I}_{1,1}) - \mathcal{I}_{1,2} + \mathcal{I}_{2,2}\,, \tag{B40}$$

$$P''_2 = \left\langle c^\dagger_{\ell\alpha} c_{\ell\alpha} c^\dagger_{\ell'\beta} c_{\ell'\beta} \right\rangle = M'^2\mathcal{I}_{2,0} + 2M'\mathcal{I}_{2,1} + \mathcal{I}_{2,2}\,, \tag{B41}$$

$$P''_3 = \left\langle c^\dagger_{\ell\alpha} c^\dagger_{\ell'\beta} c_{\ell\alpha} c_{\ell'\beta} \right\rangle = M'(M'+1)(\mathcal{I}_{1,0} - \mathcal{I}_{2,0}) + (2M'+1)(\mathcal{I}_{1,1} - \mathcal{I}_{2,1}) + \mathcal{I}_{1,2} - \mathcal{I}_{2,2}\,. \tag{B42}$$

Thus we have,

$$\begin{aligned}\langle O_2\rangle = \frac{N_2}{D} = \frac{P_0}{M}\Bigg\{1 &+ \gamma_0^2\left[\left(\frac{P_1}{P_0} - \frac{L_0}{M}\right)D_{1\phi} + \left(\frac{P_2}{P_0} - \frac{L_0}{M}\right)D_{2\phi} + \left(\frac{P_3}{P_0} - \frac{L_0}{M}\right)D_{3\phi}\right] \\ &+ g_0^2\left[\left(\frac{P'_1}{P_0} - \frac{L'_0}{M}\right)D'_{1\psi} + \left(\frac{P'_2}{P_0} - \frac{L'_0}{M}\right)D'_{2\psi} + \left(\frac{P'_3}{P_0} - \frac{L'_0}{M}\right)D'_{3\psi}\right] \\ &+ g_0^2\left[\left(\frac{P''_1}{P_0} - \frac{L''_0}{M}\right)D''_{1\psi} + \left(\frac{P''_2}{P_0} - \frac{L''_0}{M}\right)D''_{2\psi} + \left(\frac{P''_3}{P_0} - \frac{L''_0}{M}\right)D''_{3\psi}\right]\Bigg\}\,.\end{aligned} \tag{B43}$$

Similarly, it is the straightforward to write,

$$Z_c = 1 - \frac{\gamma^2}{\epsilon}P_\gamma - \frac{g^2}{2\bar{r}}P_g\,, \tag{B44}$$

where

$$P_\gamma = \frac{P_1 + P_2 - 2P_3}{P_0}\,, \tag{B45}$$

$$P_g = \frac{P'_1 + P'_2 - 2P'_3 + P''_1 + P''_2 - 2P''_3}{P_0}\,. \tag{B46}$$

Note that for $M = 2\,, M' = 1$, we obtain $P_g = 3$ and $P_\gamma = 3/4$ which agrees with the result that can be obtained from (3.31) and the results in Section III.

3. RG flow

We are now in a position to write the beta functions for the coupling constants. Using (B2) we find two equations,

$$\frac{\epsilon}{2}\gamma Z_S + \left[Z_S - \frac{\gamma}{2}\frac{\partial Z_S}{\partial \gamma}\right]\beta(\gamma) - \frac{\gamma}{2}\frac{\partial Z_S}{\partial g}\beta(g) = 0\,, \tag{B47}$$

$$\bar{r} g Z_c + \left[Z_c - \frac{g}{2}\frac{\partial Z_c}{\partial g}\right]\beta(g) - \frac{g}{2}\frac{\partial Z_c}{\partial \gamma}\beta(\gamma) = 0\,. \tag{B48}$$

We have used the exact relations $\widetilde{Z}_g = \widetilde{Z}_\gamma = 1$ in obtaining these equations. Solving these two equations and using the expressions for the renormalization factors found above we obtain the following one-loop beta functions,

$$\beta(g) = -\bar{r} g + \frac{P_g}{2} g^3 + \frac{P_\gamma}{2} g\gamma^2\,, \tag{B49}$$

$$\beta(\gamma) = -\frac{\epsilon}{2}\gamma + \frac{L_\gamma}{2}\gamma^3 + \frac{L_g}{2}\gamma g^2\,. \tag{B50}$$

Recall that at $M = 2, M' = 1$, we have $P_g = 3$, $P_\gamma = 3/4$, $L_g = 2$, and $L_\gamma = 2$. With this the above expressions match the one-loop beta functions derived earlier in Sec. III.

We can also calculate the anomalous dimension for the spin and electron operators, defined in (3.32). From (B47) and (B48) we obtain exactly the same equations derived before, *i.e.*, (3.35) and (3.37). Thus at the non-trivial fixed point where $\gamma* \neq 0, g* \neq 0$ we obtain $\eta_S = \epsilon$ and $\eta_c = 2\bar{r}$ to all orders in ϵ and $\bar{r}$.

Appendix C: Large M limit

In this appendix we consider the large M limit examined originally in the insulating spin model in Ref. 18. To extend the large M limit to the t-J model, we also need to endow the electron with an additional orbital index $\ell = 1 \ldots M'$ as in (A2), and take the large M limit at fixed

$$k \equiv \frac{M'}{M} \tag{C1}$$

using SU($M'|M$) superspin formulation of Appendix A 1 while imposing the constraint (A6) at $P = M/2$. Similar large M limits were taken in particle-hole symmetric models in Refs. [42–45] and for a non-random t-J model in Refs. [40, 41].

A sketch of our proposed large M phase diagram is shown in Fig. 8. This applies to the theory obtained by taking the large M limit of the path integral $\mathcal{Z}$ in (2.4) by inserting the SU($M'|M$) superspin operators in (A2) and (A3), and rescaling $t^2 \to t^2/M$ and $J^2 \to J^2/M$. See Ref. 45

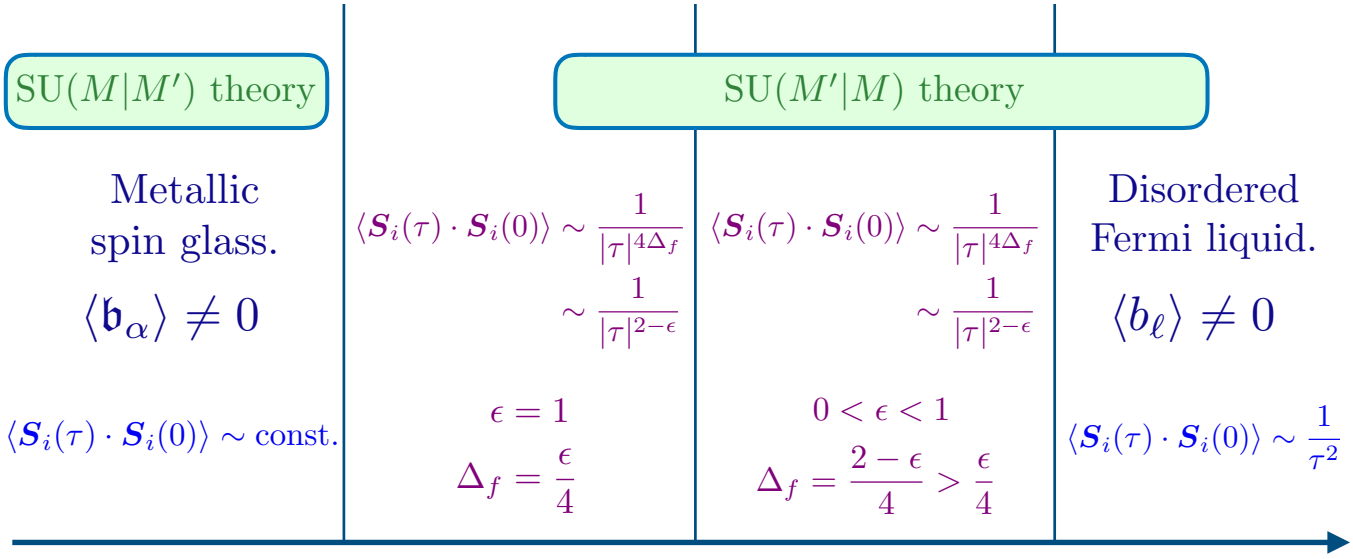

FIG. 8. Schematic phase diagram in the large M limit, with the phases displaying more rapidly decaying spin correlations as we move to the right. This appendix describes only the two intermediate critical phases in the SU($M'|M$) theory with bosonic holons and fermionic spinons. We propose in the present paper that for the case $M = 2$, $M' = 1$, these two critical phases reduce to a critical point with the characteristics of the $\epsilon = 1$ phase, as shown in Fig. 1 . A description of the spin glass phase in the large M limit requires fermionic holons and bosonic spinons in the SU($M|M'$) theory, which we do not examine here. We also note that for $M' > 1$, the disordered Fermi liquid phase also has glassy correlations associated with the 'orbital' index $\ell = 1 \ldots M'$.

for details of a similar computation with particle-hole symmetry. In our case, both the boson and fermion Green's functions will have to be particle-hole asymmetric, as in Refs. [18, 27, 28, 76].

We will perform an analytic low energy analysis of the large M equations, and find a critical solution which is in close correspondence with the RG fixed point FP_4 in Section III. However, the large M solution appears to be present for a range of dopings, and not at a critical doping as in the RG analysis. We expect that either constraints from the higher energy structure of the large M theory, or corrections higher order in $1/M$, will convert the critical phase to a critical point. It appears that the numerical studies of Haule *et al.* [40, 41] examined the finite temperature behavior about the critical phase described here as their model of the pseudogap. This contrasts with our model of the pseudogap in Fig. 1 as a metallic spin glass flanking a critical point. We also note that the present large M limit, with fermionic spinons, cannot obtain a metallic spin glass; instead we have to use the bosonic spinon approach outlined in Section IV B.

1. Green's functions

We follow the condensed matter notation for Green's functions in which

$$G_f(\tau) = -\langle T_\tau(f(\tau)f^\dagger(0))\rangle, \tag{C2}$$

$$G_b(\tau) = -\langle T_\tau(b(\tau)b^\dagger(0))\rangle. \tag{C3}$$

We drop indices α, ℓ, and all Green's functions are diagonal in these indices. It is useful to make ansatzes for the retarded Green's functions in the complex frequency plane, because then the constraints from the positivity of the spectral weight are clear. At the Matsubara frequencies, the Green's function is defined by

$$G(i\omega_n) = \int_0^{1/T} d\tau e^{i\omega_n\tau} G(\tau). \tag{C4}$$

So the bare Green's functions are

$$G_{f0}(i\omega_n) = \frac{1}{i\omega_n - \mu_f} \tag{C5}$$

$$G_{b0}(i\omega_n) = \frac{1}{i\omega_n - \mu_b}\,. \tag{C6}$$

The Green's functions are continued to all complex frequencies z via the spectral representation

$$G(z) = \int_{-\infty}^{\infty} \frac{d\Omega}{\pi} \frac{\rho(\Omega)}{z - \Omega}. \tag{C7}$$

For fermions, the spectral density obeys

$$\rho_f(\Omega) > 0, \tag{C8}$$

for all real Ω and T, and for bosons the constraint is

$$\Omega\, \rho_b(\Omega) > 0. \tag{C9}$$

The retarded Green's function is $G^R(\omega) = G(\omega + i\eta)$ with η a positive infinitesimal, while the advanced Green's function is $G^A(\omega) = G(\omega - i\eta)$. It is also useful to tabulate the inverse Fourier transforms at $T = 0$

$$G(\tau) = \begin{cases} -\displaystyle\int_0^\infty \frac{d\Omega}{\pi} \rho(\Omega) e^{-\Omega\tau} & \text{, for } \tau > 0 \text{ and } T = 0 \\ \displaystyle\int_0^\infty \frac{d\Omega}{\pi} \rho(-\Omega) e^{\Omega\tau} & \text{, for } \tau < 0 \text{ and } T = 0 \end{cases}. \tag{C10}$$

2. Saddle point and self-consistency equations

The saddle-point equations of the SU($M'|M$) form of (2.4), after rescaling $t^2 \to t^2/M$ and $J^2 \to J^2/M$, for the boson and fermion Green's functions are

$$G_b(i\omega_n) = \frac{1}{i\omega_n + \mu_b - \Sigma_b(i\omega_n)}, \quad \Sigma_b(\tau) = t^2 G_f(\tau) R(-\tau) \tag{C11}$$

$$G_f(i\omega_n) = \frac{1}{i\omega_n + \mu_f - \Sigma_f(i\omega_n)}, \quad \Sigma_f(\tau) = J^2 G_f(\tau) Q(\tau) - k\, t^2 R(\tau) G_b(\tau)\,, \tag{C12}$$

while the self-consistency equations in (2.3) are

$$R(\tau) = -G_f(\tau) G_b(-\tau) \quad , \quad Q(\tau) = -G_f(\tau) G_f(-\tau) \tag{C13}$$

Here μ_f and μ_b are chemical potentials, determined by ϵ_0 and the saddle point value of λ, and chosen to satisfy

$$\left\langle f^\dagger f \right\rangle = \frac{1}{2} - kp \quad , \quad \left\langle b^\dagger b \right\rangle = p\,. \tag{C14}$$

Eqs. (C12,C13,C14) are identical to the ones considered in Refs [40, 41] as an EDMFT approximation to the non-random t-J model. We will look for gapless critical solutions of the above equations. We expect that such solutions exist only for $p < p_c$, and that for $p > p_c$ the boson condenses, leading to a Fermi liquid solution.

3. Low frequency ansatzes

For the fermion Green's function, we write at a complex frequency $|z| \ll J$

$$G_f(z) = C_f \frac{e^{-i(\pi\Delta_f + \theta_f)}}{z^{1-2\Delta_f}} \quad , \quad \mathrm{Im}(z) > 0, \tag{C15}$$

which is expressed in terms of three real parameters, C_f, Δ_f and θ_f. Then the constraint (C8) becomes

$$\sin(\pi\Delta_f + \theta_f) > 0 \quad , \quad \sin(\pi\Delta_f - \theta_f) > 0. \tag{C16}$$

The particle-hole symmetric value is $\theta_f = 0$. Using (C10) we obtain in τ space for $|\tau| \gg 1/J$

$$G_f(\tau) = \begin{cases} -\dfrac{C_f \Gamma(2\Delta_f)\sin(\pi\Delta_f + \theta_f)}{\pi |\tau|^{2\Delta_f}} & , \text{ for } \tau > 0 \text{ and } T = 0 \\ \dfrac{C_f \Gamma(2\Delta_f)\sin(\pi\Delta_f - \theta_f)}{\pi |\tau|^{2\Delta_f}} & , \text{ for } \tau < 0 \text{ and } T = 0 \end{cases} . \tag{C17}$$

We can also write corresponding ansatz for the fermionic correlator $R(\tau)$, which we will only need as a function of τ for $|\tau| \gg 1/J$

$$R(\tau) = \begin{cases} -\dfrac{C_{+R}}{|\tau|^{2(1-\bar{r})}} & , \text{ for } \tau > 0 \text{ and } T = 0 \\ \dfrac{C_{-R}}{|\tau|^{2(1-\bar{r})}} & , \text{ for } \tau < 0 \text{ and } T = 0 \end{cases} . \tag{C18}$$

where $C_{+R} > 0$ and $C_{-R} > 0$, but they need not be equal. This corresponds to the ansatz in (2.8) which has $C_{+R} = C_{-R}$. We can allow these amplitudes to be distinct in the large M limit. We also examined generalization of the RG analysis in Section III to the case $C_{+R} \neq C_{-R}$; we found that the perturbative RG then gave inconsistent renormalizations of the coupling g, and so $C_{+R} = C_{-R}$ in the context of the ϵ and $\bar{r}$ expansion.

For the boson Green's function, we write at a complex frequency $|z| \ll J$

$$G_b(z) = C_b \frac{e^{-i(\pi\Delta_b + \theta_b)}}{z^{1-2\Delta_b}} \quad , \quad \mathrm{Im}(z) > 0, \tag{C19}$$

expressed in terms of the three real parameters, C_b, Δ_b and θ_b. The constraint (C9) becomes

$$\sin(\pi\Delta_b + \theta_b) > 0 \quad , \quad \sin(\pi\Delta_b - \theta_b) < 0. \tag{C20}$$

Using (C10) we obtain in τ space for $|\tau| \gg 1/J$

$$G_b(\tau) = \begin{cases} -\dfrac{C_b \Gamma(2\Delta_b)\sin(\pi\Delta_b + \theta_b)}{\pi |\tau|^{2\Delta_b}} & , \text{ for } \tau > 0 \text{ and } T = 0 \\ \dfrac{C_b \Gamma(2\Delta_b)\sin(\pi\Delta_b - \theta_b)}{\pi |\tau|^{2\Delta_b}} & , \text{ for } \tau < 0 \text{ and } T = 0 \end{cases} . \tag{C21}$$

Finally, we can write expressions similar to (C18) for $Q(\tau)$ for $|\tau| \gg 1/J$

$$Q(\tau) = \begin{cases} \dfrac{C_Q}{|\tau|^{2-\epsilon}} & , \text{ for } \tau > 0 \text{ and } T = 0 \\ \dfrac{C_Q}{|\tau|^{2-\epsilon}} & , \text{ for } \tau < 0 \text{ and } T = 0 \end{cases} . \tag{C22}$$

where $C_Q > 0$. This corresponds to the ansatz for $Q(\tau)$ in (2.8)

We can relate the parameters in the ansatzes for the bosonic bath $Q(\tau)$ and the fermionic bath $R(\tau)$ to the parameters in the ansatzes for the Green's functions G_f and G_b, by using the self-consistency conditions (C13). This yields expressions for $\bar{r}$, ϵ, $C_{\pm R}$, and C_Q in terms of $\Delta_{f,b}$, $\theta_{f,b}$, and $C_{f,b}$:

$$\begin{aligned} \bar{r} &= 1 - \Delta_f - \Delta_b \\ \epsilon &= 2(1 - 2\Delta_f) \\ C_{+R} &= -\frac{C_f C_b \Gamma(2\Delta_f)\Gamma(2\Delta_b)\sin(\pi\Delta_f + \theta_f)\sin(\pi\Delta_b - \theta_b)}{\pi^2} \\ C_{-R} &= \frac{C_f C_b \Gamma(2\Delta_f)\Gamma(2\Delta_b)\sin(\pi\Delta_f - \theta_f)\sin(\pi\Delta_b + \theta_b)}{\pi^2} \\ C_Q &= \frac{[C_f \Gamma(2\Delta_f)]^2 \sin(\pi\Delta_f + \theta_f)\sin(\pi\Delta_f - \theta_f)}{\pi^2} . \end{aligned} \tag{C23}$$

However, in keeping with RG computation, we will defer application of the relations in (C23).

4. Luttinger constraints

The Luttinger constraints on the spectral asymmetries of the Green's functions are very similar to those in Refs. [28, 77], and can be obtained by the method of Ref. 78:

$$\frac{\theta_f}{\pi} + \left(\frac{1}{2} - \Delta_f\right) \frac{\sin(2\theta_f)}{\sin(2\pi\Delta_f)} = kp$$
$$\frac{\theta_b}{\pi} + \left(\frac{1}{2} - \Delta_b\right) \frac{\sin(2\theta_b)}{\sin(2\pi\Delta_b)} = \frac{1}{2} + p\,.$$

These constraints imply $-\pi\Delta_f < \theta_f < \pi\Delta_f$ and $\pi\Delta_b < \theta_b < \pi/2$. The determine the spectral asymmetry angles $\theta_{f,b}$ in terms of the density p and the scaling dimensions $\Delta_{f,b}$.

5. Self-energies

We can now collect the corresponding expressions for the fermionic and bosonic self energies at $|\tau| \gg 1/J$ and $T = 0$:

$$\Sigma_f(\tau) = -kt^2 \left[\frac{C_b C_{+R}\Gamma(2\Delta_b)}{\pi}\right] \frac{\sin(\pi\Delta_b + \theta_b)}{|\tau|^{2\Delta_b + 2(1-\bar{r})}} - J^2 \left[\frac{C_f C_Q \Gamma(2\Delta_f)}{\pi}\right] \frac{\sin(\pi\Delta_f + \theta_f)}{|\tau|^{2\Delta_f + 2 - \epsilon}}, \quad \tau > 0 \tag{C24}$$

$$\Sigma_f(\tau) = -kt^2 \left[\frac{C_b C_{-R}\Gamma(2\Delta_b))}{\pi}\right] \frac{\sin(\pi\Delta_b - \theta_b)}{|\tau|^{2\Delta_b + 2(1-\bar{r})}} + J^2 \left[\frac{C_f C_Q \Gamma(2\Delta_f)}{\pi}\right] \frac{\sin(\pi\Delta_f - \theta_f)}{|\tau|^{2\Delta_f + 2 - \epsilon}}, \quad \tau < 0 \tag{C25}$$

$$\Sigma_b(\tau) = -t^2 \left[\frac{C_f C_{-R}\Gamma(2\Delta_f)}{\pi}\right] \frac{\sin(\pi\Delta_f + \theta_f)}{|\tau|^{2\Delta_f + 2(1-\bar{r})}}, \quad \tau > 0 \tag{C26}$$

$$\Sigma_b(\tau) = -t^2 \left[\frac{(C_f C_{+R}\Gamma(2\Delta_f)}{\pi}\right] \frac{\sin(\pi\Delta_f - \theta_f)}{|\tau|^{2\Delta_f + 2(1-\bar{r})}}, \quad \tau < 0 \tag{C27}$$

We also use the spectral representations for the self energies

$$\Sigma(z) = \int_{-\infty}^{\infty} \frac{d\Omega}{\pi} \frac{\sigma(\Omega)}{z - \Omega}. \tag{C28}$$

Performing the inverse of the Laplace transforms in (C10) we obtain at $T = 0$ and $|\Omega| \ll J$

$$\sigma_f(\Omega) = \frac{\pi k t^2}{\Gamma(2\Delta_b + 2(1-\bar{r}))} \left[\frac{C_b C_{+R} \Gamma(2\Delta_b)}{\pi}\right] \frac{\sin(\pi\Delta_b + \theta_b)}{|\Omega|^{1-2\Delta_b-2(1-\bar{r})}} + \frac{\pi J^2}{\Gamma(2\Delta_f + 2 - \epsilon)} \left[\frac{C_f C_Q \Gamma(2\Delta_f)}{\pi}\right] \frac{\sin(\pi\Delta_f + \theta_f)}{|\Omega|^{-1-2\Delta_f+\epsilon}}, \quad \Omega > 0 \tag{C29}$$

$$\sigma_f(\Omega) = -\frac{\pi k t^2}{\Gamma(2\Delta_b + 2(1-\bar{r}))} \left[\frac{C_b C_{-R} \Gamma(2\Delta_b)}{\pi}\right] \frac{\sin(\pi\Delta_b - \theta_b)}{|\Omega|^{1-2\Delta_b-2(1-\bar{r})}} + \frac{\pi J^2}{\Gamma(2\Delta_f + 2 - \epsilon)} \left[\frac{C_f C_Q \Gamma(2\Delta_f)}{\pi}\right] \frac{\sin(\pi\Delta_f - \theta_f)}{|\Omega|^{-1-2\Delta_f+\epsilon}}, \quad \Omega < 0 \tag{C30}$$

$$\sigma_b(\Omega) = \frac{\pi t^2}{\Gamma(2\Delta_f + 2(1-\bar{r}))} \left[\frac{C_f C_{-R} \Gamma(2\Delta_f)}{\pi}\right] \frac{\sin(\pi\Delta_f + \theta_f)}{|\Omega|^{1-2\Delta_f-2(1-\bar{r})}}, \quad \Omega > 0 \tag{C31}$$

$$\sigma_b(\Omega) = -\frac{\pi t^2}{\Gamma(2\Delta_f + 2(1-\bar{r}))} \left[\frac{C_f C_{+R} \Gamma(2\Delta_f) C_b}{\pi}\right] \frac{\sin(\pi\Delta_f - \theta_f)}{|\Omega|^{1-2\Delta_f-2(1-\bar{r})}}, \quad \Omega < 0 \tag{C32}$$

6. Solution of the saddle point equations

We will now determine the constraints placed by the saddle point equations (C11) and (C12) on the parameters of the low frequency ansatzes presented in Section C 3. As in the body of the text, we will defer application of the self-consistency conditions (C13), which led to the relations (C23). This will allow us to make a more complete comparison of the results of the large M theory with that in Section III.

From (C19) we have

$$\Sigma_b(z) = -\frac{1}{C_b} e^{i(\pi\Delta_b + \theta_b)} z^{(1-2\Delta_b)}. \tag{C33}$$

Comparing (C31), (C32) and (C33) we have the exponent identity

$$\Delta_f + \Delta_b = \bar{r}\,. \tag{C34}$$

In the present large M limit, the electron Green's function is given by

$$G_c(\tau) = -G_f(\tau) G_b(-\tau)\,, \tag{C35}$$

and so the anomalous dimension of the electron operator is

$$\eta_c = 2(\Delta_f + \Delta_b)\,. \tag{C36}$$

Now we see that the large M result (C34) is precisely the result (3.38) for the electron anomalous dimension obtained to all orders in the ϵ and $\bar{r}$ expansions.

Comparing the amplitudes of (C31), (C32) and (C33) we obtain

$$\frac{\pi t^2}{\Gamma(2\Delta_f + 2(1-\bar{r}))}\left[\frac{C_f C_{-R}\Gamma(2\Delta_f)}{\pi}\right]\sin(\pi\Delta_f + \theta_f) = \frac{\sin(\pi\Delta_b + \theta_b)}{C_b} \tag{C37}$$

$$\frac{\pi t^2}{\Gamma(2\Delta_f + 2(1-\bar{r}))}\left[\frac{C_f C_{+R}\Gamma(2\Delta_f)}{\pi}\right]\sin(\pi\Delta_f - \theta_f) = -\frac{\sin(\pi\Delta_b - \theta_b)}{C_b} \tag{C38}$$

From (C15) we have

$$\Sigma_f(z) = -\frac{1}{C_f}e^{i(\pi\Delta_f+\theta_f)}z^{(1-2\Delta_f)}. \tag{C39}$$

The comparison of this with (C29), (C30) leads to two possible solutions, appearing as the two intermediate critical phases in Fig. 8.

a. $\Delta_f > \epsilon/4$

The second J^2 terms in (C29) and (C30) are much smaller than the t^2 terms when $\Delta_f - \epsilon/2 > \Delta_b - \bar{r}$; using (C34), we obtain the condition $\Delta_f > \epsilon/4$. So the J^2 terms can be neglected. Indeed, the low energy solution is then entirely independent of the strength of the exchange interaction, which is rather different from the structure of the FP_4 fixed point in Section III with both $g*$ and $\gamma*$ non-zero. Instead, it is the FP_3 fixed point, with $\gamma* = 0$, which matches the structure of the present large M solution, and this fixed point was found to be unstable in the RG analysis for $M = 2$, $M' = 1$. We will therefore only write down the saddle point equations here, and not consider this case further.

From (C39), (C29) and (C30) we have

$$\frac{\pi k t^2}{\Gamma(2\Delta_b + 2(1-\bar{r}))}\left[\frac{C_b C_{+R}\Gamma(2\Delta_b)}{\pi}\right]\sin(\pi\Delta_b + \theta_b) = \frac{\sin(\pi\Delta_f + \theta_f)}{C_f} \tag{C40}$$

$$\frac{\pi k t^2}{\Gamma(2\Delta_b + 2(1-\bar{r}))}\left[\frac{C_b C_{-R}\Gamma(2\Delta_b)}{\pi}\right]\sin(\pi\Delta_b - \theta_b) = -\frac{\sin(\pi\Delta_f - \theta_f)}{C_f} \tag{C41}$$

The combination of (C37), (C41) or (C38), (C40) yields

$$\frac{\Gamma(2\Delta_f)\sin(\pi\Delta_f + \theta_f)\sin(\pi\Delta_f - \theta_f)}{\Gamma(2\Delta_b)\sin(\pi\Delta_b + \theta_b)\sin(\pi\Delta_b - \theta_b)} = -k \tag{C42}$$

We also have from (C37), (C38) or (C40), (C41)

$$\frac{C_{+R}}{C_{-R}} = -\frac{\sin(\pi\Delta_f + \theta_f)\sin(\pi\Delta_b - \theta_b)}{\sin(\pi\Delta_f - \theta_f)\sin(\pi\Delta_b + \theta_b)} \tag{C43}$$

which is consistent with the relations in (C23).

We can also apply the self-consistency relations in (C23) to the exponents, and obtain $\bar{r} = 1/2$ and $\Delta_f = (2-\epsilon)/4$.

b. $\Delta_f = \epsilon/4$

Now the t^2 and J^2 terms in (C29) and (C30) are equally important, and we will see that the structure of this large M solution is very similar to that of the critical point found in the RG analysis in Section III.

Solving (C34) and $\Delta_f - \epsilon/2 = \Delta_b - \bar{r}$ we obtain the scaling dimensions.

$$\Delta_f = \frac{\epsilon}{4} \tag{C44}$$

$$\Delta_b = \bar{r} - \frac{\epsilon}{4} \tag{C45}$$

In the large M limit, the spin correlator is given by

$$\langle \boldsymbol{S}(\tau) \cdot \boldsymbol{S}(0) \rangle \sim -G_f(\tau) G_f(-\tau) \tag{C46}$$

and so the anomalous dimension of the spin operator is

$$\eta_S = 4\Delta_f \tag{C47}$$

We now see that the spin anomalous dimension implied by the large M equations (C44) and (C47) is consistent with the result (3.36) obtained to all orders in the ϵ and $\bar{r}$ expansion.

Comparison of the amplitude of (C29) with (C39) yields

$$\begin{aligned} & kt^2 \frac{C_b C_{+R} \Gamma(2\bar{r} - \epsilon/2)}{\Gamma(2 - \epsilon/2)} \sin(\pi\Delta_b + \theta_b) \\ & \quad + J^2 \frac{C_f C_Q \Gamma(\epsilon/2)}{\Gamma(2 - \epsilon/2)} \sin(\pi\Delta_f + \theta_f) = \frac{\sin(\pi\Delta_f + \theta_f)}{C_f} \end{aligned} \tag{C48}$$

while the comparison of (C30) with (C39) yields

$$\begin{aligned} & -kt^2 \frac{C_b C_{-R} \Gamma(2\bar{r} - \epsilon/2)}{\Gamma(2 - \epsilon/2)} \sin(\pi\Delta_b - \theta_b) \\ & \quad + J^2 \frac{C_f C_Q \Gamma(\epsilon/2)}{\Gamma(2 - \epsilon/2)} \sin(\pi\Delta_f - \theta_f) = \frac{\sin(\pi\Delta_f - \theta_f)}{C_f} \end{aligned} \tag{C49}$$

Comparison of (C48) and (C49) again yields (C43), which is consistent with (C23).

Let us combine the saddle point equations (C37), (C38), (C44), (C45), (C48), and (C49) with self-consistency equations (C23), and collect all the equations which determine the parameters $\Delta_{f,b}$, $\theta_{f,b}$, and $C_{f,b}$ in the low frequency ansatzes for G_f and G_b in (C15) and (C19). All these equations reduce to $\epsilon = 1$, $\bar{r} = 1/2$, and the following independent equations

$$\begin{aligned} \Delta_f &= \frac{1}{4} \\ \Delta_b &= \frac{1}{4} \\ t^2 C_f^2 C_b^2 \cos(2\theta_f) &= \pi \\ J^2 C_f^4 \cos(2\theta_f) - kt^2 C_f^2 C_b^2 \cos(2\theta_b) &= \pi \,. \end{aligned} \tag{C50}$$

Note that the values of Δ_f and Δ_b above, combined with (C36) and (C47) yield the self-consistent values in (3.39). For the last two equations in (C50), notice the bounds $|\theta_f| < \pi/4$ and $\pi/4 < \theta_b < \pi/2$ below (C24); so all the co-efficients on the left hand sides of (C50) are positive, and the last two equations determine the values of C_f and C_b. The values of θ_f and θ_b are then determined by the particle density p from (C24). So this low energy solution can exist at a variable particle density, and the present low energy $M = \infty$ theory describes a potential critical phase, rather than a critical point.

Finally, let us note the form of the electron Green's function from (C35)

$$G_c(\tau) = \begin{cases} \dfrac{C_f C_b \sin(\pi/4 + \theta_f)\sin(\pi/4 - \theta_b)}{\pi|\tau|} & , \text{ for } \tau > 0 \text{ and } T = 0 \\ \dfrac{C_f C_b \sin(\pi/4 - \theta_f)\sin(\pi/4 + \theta_b)}{\pi|\tau|} & , \text{ for } \tau < 0 \text{ and } T = 0 \end{cases} . \tag{C51}$$

The exponent and signs of (C51) agree with the self-consistent electron Green's function obtained in (3.40) (recall (C16) and (C20)), but it appears that the magnitudes of the amplitudes in (C51) can be different between $\tau > 0$ and $\tau < 0$. This is a subtle feature of the large M theory which is not reproduced by the ϵ and $\bar{r}$ expansion in the body of the paper. This is related to the discussion below (C18).

Also note that the $1/\tau$ decay of (C51) is similar to that of a Fermi liquid. Nevertheless, this state is not a Fermi liquid because the spin correlator in (C46) decays as $1/|\tau|$, in contrast to the $1/\tau^2$ decay expected in a Fermi liquid. The exponents in (C46) and (C51) can be understood together in a picture of fractionalization of the electron into spinons and holons, where the spinon and holon correlators both decay as $1/\sqrt{\tau}$.

Appendix D: RG details

This appendix contains further details on the RG computation of Section III.

The beta functions are defined as follows:

$$\beta(g) = \mu \frac{dg}{d\mu}|_{g_0} ; \qquad \beta(\gamma) = \mu \frac{d\gamma}{d\mu}|_{\gamma_0} \tag{D1}$$

To begin,

$$\mu \frac{dg_0}{d\mu} = 0 = \bar{r}\frac{\mu^{\bar{r}} Z_g g}{\sqrt{Z_f Z_b}} + \mu \frac{\mu^{\bar{r}} g}{\sqrt{Z_f Z_b}} \frac{dZ_g}{d\mu} + \mu \frac{\mu^{\bar{r}} Z_g}{\sqrt{Z_f Z_b}} \frac{dg}{d\mu} - \frac{\mu}{2} \frac{\mu^{\bar{r}} Z_g g}{\sqrt{Z_f Z_b}} \left[\frac{1}{Z_f}\frac{dZ_f}{d\mu} + \frac{1}{Z_b}\frac{dZ_b}{d\mu} \right] , \tag{D2}$$

which gives us,

$$\begin{aligned} &\bar{r} g Z_g Z_f Z_b + \beta(g) \left[Z_g Z_f Z_b + g Z_f Z_b \frac{\partial Z_g}{\partial g} - \frac{g}{2}\left(Z_g Z_b \frac{\partial Z_f}{\partial g} + Z_g Z_f \frac{\partial Z_b}{\partial g} \right) \right] \\ &+ \beta(\gamma) \left[g Z_f Z_b \frac{\partial Z_g}{\partial \gamma} - \frac{g}{2}\left(Z_g Z_b \frac{\partial Z_f}{\partial \gamma} + Z_g Z_f \frac{\partial Z_b}{\partial \gamma} \right) \right] = 0 . \end{aligned} \tag{D3}$$

Similarly, we have

$$\frac{\epsilon}{2}\gamma Z_\gamma Z_f + \beta(g)\gamma\left[Z_f\frac{\partial Z_\gamma}{\partial g} - Z_\gamma\frac{\partial Z_f}{\partial g}\right] + \beta(\gamma)\left[\gamma Z_f\frac{\partial Z_\gamma}{\partial \gamma} + Z_f Z_\gamma - \gamma Z_\gamma\frac{\partial Z_f}{\partial \gamma}\right] = 0\,. \tag{D4}$$

1. Flow away from criticality

For the flow equation of s at one-loop, we will follow the momentum-shell RG procedure, where the cut-off D is kept explicitly. In this case, we introduce masses for bosons and fermions, but keeping in mind that only their difference is physically relevant. To this end we consider the Fourier-transformed action,

$$\begin{aligned} S(D-\delta D) &= S_\psi(D-\delta D) + S_g(D-\delta D) + S_\gamma(D-\delta D) + S_\phi(D-\delta D) \\ &\quad + \frac{1}{\beta}\sum_{i\omega_n,\alpha} f_\alpha^\dagger\left[-i\omega_n + \lambda + m_f + \Sigma_F\right] f_\alpha + \frac{1}{\beta}\sum_{i\omega_n} b^\dagger\left[-i\omega_n + \lambda + m_b + \Sigma_B\right] b\,, \end{aligned} \tag{D5}$$

where the self energies are evaluated as follows:

$$\begin{aligned} \Sigma_a &= g_0^2\int_{D-\delta D}^{D} dk \frac{k^r}{i\omega_n - \lambda - k - mb} = -g_0^2 D^{r-1}\left(\delta D + (i\omega_n - \lambda - m_b)\frac{\delta D}{D}\right) \\ &= -g^2\left(\delta D + (i\omega_n - \lambda - m_b)\frac{\delta D}{D}\right) \qquad (\text{with}\ \ g^2 \equiv g_0^2 D^{r-1})\,, \end{aligned} \tag{D6}$$

$$\begin{aligned} \Sigma_b &= \gamma_0^2\frac{3}{4}\frac{S_d}{2}\int_{D-\delta D}^{D} dk \frac{k^{d-2}}{i\omega_n - \lambda - k - m_f} = -\frac{3}{4}\gamma_0^2\frac{S_d}{2}D^{d-3}\left(\delta D + (i\omega_n - \lambda - m_f)\frac{\delta D}{D}\right) \\ &= -\frac{3}{4}\gamma^2\frac{S_d}{2\widetilde{S}_{d+1}}\left(\delta D + (i\omega_n - \lambda - m_f)\frac{\delta D}{D}\right) \qquad (\text{with}\ \ \gamma^2 \equiv \gamma_0^2 D^{d-3}\widetilde{S}_{d+1})\,, \end{aligned} \tag{D7}$$

$$\begin{aligned} \Sigma_c &= 2g_0^2\int_{D-\delta D}^{D} dk \frac{k^r}{i\omega_n - \lambda - k - mb} = -2g_0^2 D^{r-1}\left(\delta D + (i\omega_n - \lambda - m_b)\frac{\delta D}{D}\right) \\ &= -2g^2\left(\delta D + (i\omega_n - \lambda - m_b)\frac{\delta D}{D}\right) \qquad (\text{with}\ \ g^2 \equiv g_0^2 D^{r-1})\,, \end{aligned} \tag{D8}$$

with $\Sigma_F = \Sigma_a + \Sigma_b$ and $\Sigma_B = \Sigma_c$. The scaling factor is $l = 1 + \delta D/D$ such that under the scaling $k' = lk$ and $i\omega' = li\omega$. Thus we have,

$$\begin{aligned} S'(D) &= l^{-3-r}(S'_c(D) + S'_g(D)) + l^{-1}S'_\gamma(D) + l^{-d+1}S'_\phi(D) \\ &\quad + \frac{l^{-2}}{\beta}\sum_{i\omega'_n} f^\dagger\left[(-i\omega'_n + \lambda)(1 + g^2\frac{\delta D}{D} + \frac{3}{4}\gamma^2\frac{\delta D}{D}) + lm_f(1 + \frac{3}{4}\gamma^2\frac{\delta D}{D}) - lg^2\delta D + lg^2 m_b\frac{\delta D}{D} - l\frac{3}{4}\gamma^2\delta D\right] f \\ &\quad + \frac{l^{-2}}{\beta}\sum_{i\omega'_n} b^\dagger\left[(-i\omega'_n + \lambda)(1 + 2g^2\frac{\delta D}{D}) + lm_b - l2g^2\delta D + l2g^2 m_f\frac{\delta D}{D}\right] b\,. \end{aligned} \tag{D9}$$

Thus we have the following expressions for the renormalized masses:

$$m_f' = \left(1 + \frac{\delta D}{D} - g^2\frac{\delta D}{D}\right) m_f - \left(g^2 + \frac{3}{4}\gamma^2\right)\frac{\delta D}{D} + g^2 m_b \frac{\delta D}{D}\,, \tag{D10}$$

$$m_b' = \left(1 + \frac{\delta D}{D} - 2g^2\frac{\delta D}{D}\right) m_b - 2g^2\frac{\delta D}{D} + 2g^2 m_f \frac{\delta D}{D}\,. \tag{D11}$$

Note that along with this the fermionic and bosonic operators, bosonic field and the coupling constants are also renormalized. For instance, $f' = l^{-1+g^2/2+3\gamma^2/8} f$ and $b' = l^{-1+g^2} b$. In addition to the self-energy corrections there is also a vertex correction to γ at this order. However, this does not influence the mass renormalization and thus we can already proceed to calculate the flow equation for the mass. In our notation introduced earlier, $s \equiv m_f - m_b$. Now,

$$\beta(s) \equiv -D\frac{\delta s}{\delta D} = -s + 3g^2 s - g^2 + \frac{3}{4}\gamma^2\,. \tag{D12}$$

We can compute the relevant eigenvalue associated with the flow of s at the fixed points of the beta functions, and find

$$\lambda_s = 1 + \frac{3\epsilon - 16\bar{r}}{6}\,, \tag{D13}$$

at the non-trivial fixed point FP_4. At the self-consistent values, *i.e.*, $\epsilon = 1$ and $\bar{r} = 1/2$ we have $\lambda_s = 1/6$, although we cannot trust the result at such large values of ϵ and $\bar{r}$. Similarly, at FP_1, FP_2, and FP_3 we find λ_s to be 1, 1, and $1 - 2\bar{r}$ respectively.

Within the momentum-shell RG, we get the same beta functions for g and γ, after considering the vertex correction as well.

2. Particle density

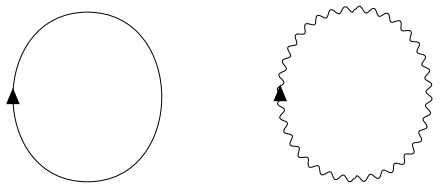

FIG. 9. Lowest order diagrams for particle densities. There are corrections, which are expected to vanish at $T = 0$.

We can also calculate the particle densities ($n_{f/b}$). This can be done at any s. We will first make the following identification: $s = \tilde{s}/\beta$, such that $\tilde{s}$ is small. This will facilitate us to do a

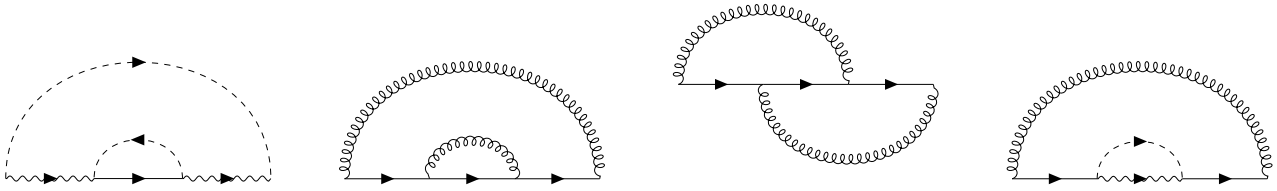

FIG. 10. Two-loop diagrams for fermion self energy. In these diagrams, solid line is for f propagator, dashed line is for ψ propagator, wavy is for b propagator, and spiral is for ϕ propagator.

small $\tilde{s}$ expansion. From the diagrams we find,

$$q_f(\lambda) = 2e^{-\beta(\lambda+s)} \sim 2e^{-\beta\lambda}(1-\tilde{s})\,, \tag{D14}$$

$$q_b(\lambda) = e^{-\beta\lambda}\,. \tag{D15}$$

$q(\lambda) = q_f(\lambda) + q_b(\lambda)$, such that,

$$n_{f/b} = \lim_{\lambda\to\infty} \frac{q_{f/b}}{q}\,. \tag{D16}$$

So, we have,

$$n_f = \frac{2-2\tilde{s}}{3-2\tilde{s}} \sim \frac{2}{3}(1-\tilde{s})(1+\frac{2}{3}\tilde{s}) \sim \frac{2}{3} - \frac{2}{9}\tilde{s}\,, \tag{D17}$$

$$n_b = \frac{1}{3-2\tilde{s}} \sim \frac{1}{3}(1+\frac{2}{3}\tilde{s}) \sim \frac{1}{3} + \frac{2}{9}\tilde{s}\,. \tag{D18}$$

Note that we still satisfy the particle density constraint $n_f + n_b = 1$ exactly. It is also interesting to note that $n_b = 1/3$ at zeroth order, which corresponds to $p_c = 1/3$.

3. Two-loop self energy

We first evaluate the fermionic self energies to two-loop order. The relevant Feynman diagrams are shown in Fig. 10.

$$\begin{aligned}
\Sigma^f_{10(a)}(i\nu) &= -2\frac{g_0^4}{\beta^2}\sum_{i\omega_{1n},i\omega_{2n}}\int dk_1 dk_2 \frac{|k_1|^r}{i\omega_{1n}-k_1}\frac{|k_2|^r}{i\omega_{2n}-k_2}\frac{1}{(i\nu-i\omega_{1n}-\lambda)^2}\frac{1}{i\nu-i\omega_{1n}+i\omega_{2n}-\lambda} \\
&= 2g_0^4\int dk_1 dk_2 \frac{|k_1|^r|k_2|^r\theta(k_1)\theta(-k_2)}{(i\nu-k_1-\lambda)^2(i\nu-k_1+k_2-\lambda)} \\
&= 2g_0^4(i\nu-\lambda)^{-1+2r}\left[\frac{1}{8\bar{r}^2} - \frac{(2\pi i-1)}{4\bar{r}}\right]\,,
\end{aligned} \tag{D19}$$

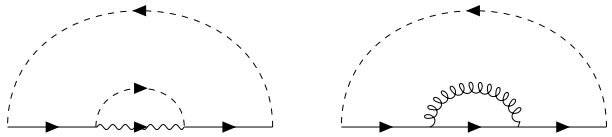

(a) (b)

FIG. 11. Two-loop diagrams for boson self energy. In these diagrams, solid line is for f propagator, dashed line is for ψ propagator, wavy is for b propagator, and spiral is for ϕ propagator.

$$\begin{aligned}\Sigma^f_{10(b)}(i\nu) &= \frac{9}{16}\frac{\gamma_0^4}{\beta^2}\sum_{i\omega_{1n},i\omega_{2n}}\int d^dk_1d^dk_2\frac{1}{\omega_{1n}^2+k_1^2}\frac{1}{\omega_{2n}^2+k_2^2}\frac{1}{(i\nu+i\omega_{1n}-\lambda)^2}\frac{1}{i\nu+i\omega_{1n}+i\omega_{2n}-\lambda}\\ &= \frac{9}{16}\gamma_0^4\int d^dk_1\frac{d^dk_2}{4k_1k_2}\frac{1}{(i\nu-k_1-\lambda)^2}\frac{1}{i\nu-k_1-k_2-\lambda}\\ &= \frac{9}{16}\gamma_0^4(i\nu-\lambda)^{-5+2d}\left[\frac{1}{2\epsilon^2}-\frac{-1+\aleph+2i\pi}{2\epsilon}\right], \end{aligned} \tag{D20}$$

$$\begin{aligned}\Sigma^f_{10(c)}(i\nu) &= \frac{-3}{16}\frac{\gamma_0^4}{\beta^2}\sum_{i\omega_{1n},i\omega_{2n}}\int d^dk_1d^dk_2\frac{1}{\omega_{1n}^2+k_1^2}\frac{1}{\omega_{2n}^2+k_2^2}\frac{1}{i\nu+i\omega_{1n}-\lambda}\frac{1}{i\nu+i\omega_{1n}+i\omega_{2n}-\lambda}\frac{1}{i\nu+i\omega_{2n}-\lambda}\\ &= \frac{-3}{16}\gamma_0^4\int d^dk_1\frac{d^dk_2}{4k_1k_2}\frac{1}{i\nu-k_1-\lambda}\frac{1}{i\nu-k_2-\lambda}\frac{1}{i\nu-k_1-k_2-\lambda}\\ &= \frac{-3}{16}\gamma_0^4(i\nu-\lambda)^{-5+2d}\left[-\frac{1}{\epsilon^2}-\frac{1-2\aleph-4i\pi}{2\epsilon}\right], \end{aligned} \tag{D21}$$

$$\begin{aligned}\Sigma^f_{10(d)}(i\nu) &= -\frac{3}{4}\frac{\gamma_0^2g_0^2}{\beta^2}\sum_{i\omega_{1n},i\omega_{2n}}\int d^dk_1dk_2|k_2|^r\frac{1}{\omega_{1n}^2+k_1^2}\frac{1}{(i\nu+i\omega_{1n}-\lambda)^2}\frac{1}{i\omega_{2n}-k_2}\frac{1}{i\nu+i\omega_{1n}-i\omega_{2n}-\lambda}\\ &= \frac{3}{4}\gamma_0^2g_0^2\int d^dk_1dk_2\frac{|k_2|^r}{2k_1}\theta(k_2)\frac{1}{(i\nu-k_1-\lambda)^2}\frac{1}{i\nu-k_1-k_2-\lambda}\\ &= \frac{3}{4}\gamma_0^2g_0^2(i\nu-\lambda)^{-3+d+r}\left[\frac{1}{2\bar{r}(\epsilon+2\bar{r})}+\frac{-2i\pi(\epsilon+2\bar{r})-\aleph\epsilon+4\bar{r}}{4\bar{r}(\epsilon+2\bar{r})}\right]. \end{aligned} \tag{D22}$$

We will now evaluate the bosonic self energies to two-loop order. The relevant Feynman diagrams are shown in Fig. 11.

$$\begin{aligned}\Sigma^b_{11(a)}(i\nu) &= -2\frac{g_0^4}{\beta^2}\sum_{i\omega_{1n},i\omega_{2n}}\int dk_1dk_2\frac{|k_1|^r}{i\omega_{1n}-k_1}\frac{|k_2|^r}{i\omega_{2n}-k_2}\frac{1}{(i\nu+i\omega_{1n}-\lambda)^2}\frac{1}{i\nu+i\omega_{1n}-i\omega_{2n}-\lambda}\\ &= 2g_0^4\int dk_1dk_2\frac{\theta(-k_1)\theta(k_2)|k_1|^r|k_2|^r}{(i\nu+k_1-\lambda)^2(i\nu+k_1-k_2-\lambda)}\\ &= 2g_0^4(i\nu-\lambda)^{-1+2r}\left[\frac{1}{8\bar{r}^2}-\frac{2i\pi-1}{4\bar{r}}\right], \end{aligned} \tag{D23}$$

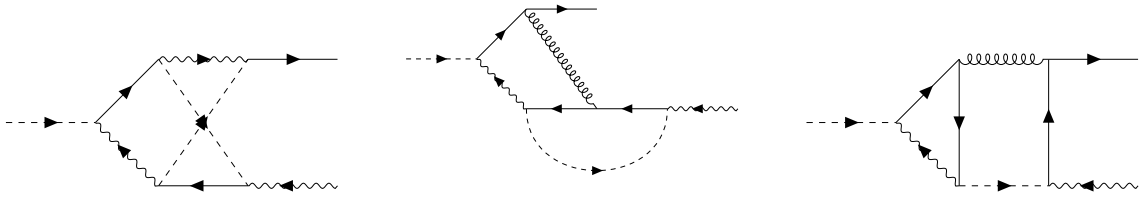

(a) (b) (c)

FIG. 12. Two-loop diagrams for vertex corrections to g_0. In these diagrams, solid line is for f propagator, dashed line is for ψ propagator, wavy is for b propagator, and spiral is for ϕ propagator.

$$\begin{aligned}\Sigma^b_{11(b)}(i\nu) &= 2\frac{3}{4}\frac{g_0^2\gamma^2}{\beta^2}\sum_{i\omega_{1n},i\omega_{2n}}\int dk_1 d^d k_2 \frac{|k_1|^r}{i\omega_{1n}-k_1}\frac{1}{\omega_{2n}^2+k_2^2}\frac{1}{(i\nu+i\omega_{1n}-\lambda)^2}\frac{1}{i\nu+i\omega_{1n}+i\omega_{2n}-\lambda} \\ &= 2\frac{3}{4}g_0^2\gamma^2\int dk_1 d^d k_2 \frac{\theta(-k_1)}{2k_2}\frac{|k_1|^r}{(i\nu+k_1-\lambda)^2(i\nu+k_1-k_2-\lambda)} \\ &= 2\frac{3}{4}g_0^2\gamma^2(i\nu-\lambda)^{-3+d+r}\left[\frac{1}{\epsilon(\epsilon+2\bar{r})}+\frac{-2i\pi(\epsilon+2\bar{r})-\aleph\epsilon+2\epsilon}{2\epsilon(\epsilon+2\bar{r})}\right]. \end{aligned} \tag{D24}$$

4. Two-loop vertex corrections

Let us first evaluate the vertex correction to the fermionic bath coupling g_0 at two-loop level. The relevant Feynman diagrams are shown in Fig. 12,.

$$\begin{aligned}\Gamma^g_{12(a)} &= \frac{g_0^5}{\beta^2}\sum_{i\omega_{1n},i\omega_{2n}}\int dk_1 dk_2 \frac{|k_1|^r}{i\Omega_{1n}-i\omega_{1n}-k_1}\frac{|k_2|^r}{i\omega_{2n}-i\Omega_{2n}-k_2} \\ &\qquad\times\frac{1}{i\omega_{1n}-\lambda}\frac{1}{i\omega_{2n}-\lambda}\frac{1}{i\omega_{2n}-i\Omega_{1n}+i\omega_{1n}-\lambda}\frac{1}{i\omega_{2n}-i\Omega_{2n}+i\omega_{1n}-\lambda} \\ &= -g_0^5\int dk_1 dk_2 \frac{|k_1|^r\theta(k_1)}{i\Omega_{1n}-k_1-\lambda}\frac{|k_2|^r\theta(-k_2)}{i\Omega_{2n}+k_2-\lambda}\frac{1}{i\Omega_{2n}+k_2-k_1-\lambda}\frac{1}{i\Omega_{1n}+k_2-k_1-\lambda}\end{aligned}$$

We set the external frequency of c particle to zero. In other words, $\Omega_{1n}=\Omega_{2n}$. Then

$$\begin{aligned}\Gamma^g_{12(a)} &= -g_0^5\int dk_2 \frac{|k_2|^r\theta(-k_2)}{i\Omega_{1n}+k_2-\lambda}\left[\frac{\pi\csc(\pi r)(l-i\Omega_{1n})^r}{k_2^2}-\frac{\pi(\lambda-i\Omega_{1n})\csc(\pi r)(-k_2+\lambda-i\Omega_{1n})^{r-1}}{k_2^2}\right. \\ &\qquad\left.-\frac{\pi(r-1)\csc(\pi r)(-k_2+\lambda-i\Omega_{1n})^{r-1}}{k_2^2}\right] \\ &= -g_0 A_\mu g^4\left[\left(\frac{1}{4\bar{r}^2}-\frac{2i\pi}{2\bar{r}}\right)-\left(\frac{1}{4\bar{r}^2}+\frac{\gamma_E-2i\pi+\log(4)+\psi^{(0)}\left(\frac{1}{2}\right)}{2\bar{r}}\right)+\frac{1}{4\bar{r}}\right] \\ &= -g_0 A_\mu g^4\left[\frac{1}{4\bar{r}}\right],\end{aligned} \tag{D25}$$

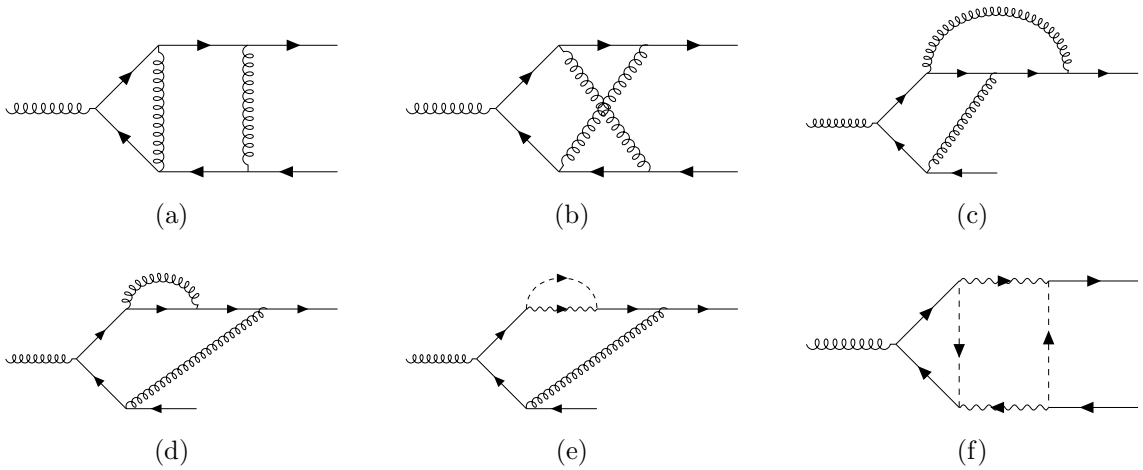

FIG. 13. Two-loop diagrams for vertex corrections to γ_0. In these diagrams, solid line is for f propagator, dashed line is for ψ propagator, wavy is for b propagator, and spiral is for ϕ propagator.

where we used $\gamma_E + \log(4) + \psi^{(0)}\left(\frac{1}{2}\right) = 0$.

$$\Gamma^g_{12(b)} = g_0 C_{s1} \frac{g_0^2\gamma_0^2}{\beta^2} \sum_{i\omega_{1n}, i\omega_{2n}} \int dk_1 d^d k_2 \frac{|k_1|^r}{i\omega_{1n} - k_1} \frac{1}{\omega_{2n}^2 + k_2^2} \frac{1}{i\Omega_{1n} + i\omega_{1n} - \lambda} \frac{1}{i\Omega_{1n} + i\omega_{1n} + i\omega_{2n} - \lambda} \times \frac{1}{i\Omega_{1n} + i\omega_{2n} - \lambda} \frac{1}{i\Omega_{2n} + i\omega_{2n} - \lambda}$$

Note that $i\Omega_{1n,2n}$ is external bosonic (fermionic) freq., $i\omega_{1n,2n}$ is internal fermionic (bosonic) freq.

$$= g_0 C_{s1} g_0^2 \gamma_0^2 \int dk_1 \frac{d^d k_2}{2k_2} \frac{|k_1|^r \theta(-k_1)}{i\Omega_{1n} + k_1 - \lambda} \frac{1}{i\Omega_{1n} - k_2 - \lambda} \frac{1}{i\Omega_{2n} - k_2 - \lambda} \frac{1}{i\Omega_{1n} + k_1 - k_2 - \lambda}\,, \tag{D26}$$

$$\Gamma^g_{12(c)} = g_0 C_{s2} \frac{g_0^2\gamma_0^2}{\beta^2} \sum_{i\omega_{1n}, i\omega_{2n}} \int dk_1 d^d k_2 \frac{|k_1|^r}{i\omega_{1n} - i\Omega_{1n} - k_1} \frac{1}{(\omega_{1n} - \Omega_{2n})^2 + k_2^2} \frac{1}{i\omega_{1n} - \lambda} \frac{1}{i\omega_{2n} - i\Omega_{1n} + i\Omega_{2n} - \lambda} \times \frac{1}{i\omega_{1n} + i\omega_{2n} - i\Omega_{1n} - \lambda} \frac{1}{i\omega_{2n} - \lambda}$$

$$= g_0 C_{s2} \frac{g_0^2\gamma_0^2}{\beta} \sum_{i\omega_{1n}} \int dk_1 d^d k_2 \frac{|k_1|^r}{i\omega_{1n} - i\Omega_{1n} - k_1} \frac{1}{(\omega_{1n} - \Omega_{2n})^2 + k_2^2} \frac{1}{i\omega_{1n} - \lambda} \times 0 = 0\,.$$

Note that $i\Omega_{1n,2n}$ is external bosonic (fermionic) freq., $i\omega_{1n,2n}$ is internal fermionic (bosonic) freq. (D27)

However, $C_{s1} = 0$. So there is only one non-zero contribution to the g_0 vertex correction.

We will now evaluate the two-loop vertex correction to the bosonic bath coupling γ_0. The

corresponding diagrams are shown in Fig. 13.

$$\begin{aligned}
\Gamma^{\gamma}_{13(a)} &= \gamma_0 \frac{1}{16}\frac{\gamma_0^4}{\beta^2}\sum_{i\omega_{1n},i\omega_{2n}}\int d^dk_2 d^dk_1 \frac{1}{\omega_{1n}^2+k_1^2}\frac{1}{\omega_{2n}^2+k_2^2}\frac{1}{i\Omega_{1n}+i\omega_{1n}-\lambda}\frac{1}{i\Omega_{1n}+i\omega_{1n}+i\omega_{2n}-\lambda} \\
&\qquad \times \frac{1}{i\Omega_{2n}+i\omega_{1n}+i\omega_{2n}-\lambda}\frac{1}{i\Omega_{2n}+i\omega_{1n}-\lambda} \\
&= \gamma_0 \frac{1}{16}\gamma_0^4 \int \frac{d^dk_2 d^dk_1}{4k_1k_2}\frac{1}{i\Omega_{1n}-k_1-k_2-\lambda}\frac{1}{i\Omega_{2n}-k_1-k_2-\lambda}\frac{1}{i\Omega_{1n}-k_1-\lambda}\frac{1}{i\Omega_{2n}-k_1-\lambda} \\
&= \gamma_0 \frac{1}{16}B_\mu\gamma^4\left(\frac{S_d}{2\widetilde{S}_{d+1}}\right)^2 \frac{\pi(-1)^{2d-6}(d-2)\csc(\pi d)\Gamma(6-2d)\Gamma(d-1)}{\Gamma(5-d)} \\
&= \gamma_0 \frac{1}{16}B_\mu\gamma^4\left[\frac{1}{2\epsilon^2}-\frac{3+\aleph+2i\pi}{2\epsilon}\right], \qquad \text{(D28)}
\end{aligned}$$

$$\begin{aligned}
\Gamma^{\gamma}_{13(b)} &= \gamma_0 \frac{5}{16}\frac{\gamma_0^4}{\beta^2}\sum_{i\omega_{1n},i\omega_{2n}}\int d^dk_2 d^dk_1 \frac{1}{\omega_{1n}^2+k_1^2}\frac{1}{\omega_{2n}^2+k_2^2}\frac{1}{i\Omega_{1n}+i\omega_{1n}-\lambda}\frac{1}{i\Omega_{1n}+i\omega_{1n}+i\omega_{2n}-\lambda} \\
&\qquad \times \frac{1}{i\Omega_{2n}+i\omega_{1n}+i\omega_{2n}-\lambda}\frac{1}{i\Omega_{2n}+i\omega_{2n}-\lambda} \\
&= \gamma_0 \frac{5}{16}\gamma_0^4 \int \frac{d^dk_2 d^dk_1}{4k_1k_2}\frac{1}{i\Omega_{1n}-k_1-k_2-\lambda}\frac{1}{i\Omega_{2n}-k_1-k_2-\lambda}\frac{1}{i\Omega_{1n}-k_1-\lambda}\frac{1}{i\Omega_{2n}-k_2-\lambda} \\
&= \gamma_0 \frac{5}{16}B_\mu\gamma^4\left(\frac{S_d}{2\widetilde{S}_{d+1}}\right)^2 \frac{\pi(-1)^{2d-6}\csc(\pi d)((d-1)\Gamma(6-2d)\Gamma(d-3)+\pi\csc(\pi d)\Gamma(3-d))}{\Gamma(3-d)} \\
&= \gamma_0 \frac{5}{16}B_\mu\gamma^4\left[\frac{1}{2\epsilon}\right], \qquad \text{(D29)}
\end{aligned}$$

$$\begin{aligned}
\Gamma^{\gamma}_{13(c)} &= \gamma_0 2\frac{1}{16}\frac{\gamma_0^4}{\beta^2}\sum_{i\omega_{1n},i\omega_{2n}}\int d^dk_2 d^dk_1 \frac{1}{\omega_{1n}^2+k_1^2}\frac{1}{\omega_{2n}^2+k_2^2}\frac{1}{i\Omega_{1n}+i\omega_{1n}-\lambda}\frac{1}{i\Omega_{1n}+i\omega_{1n}+i\omega_{2n}-\lambda} \\
&\qquad \times \frac{1}{i\Omega_{1n}+i\omega_{2n}-\lambda}\frac{1}{i\Omega_{2n}+i\omega_{2n}-\lambda}
\end{aligned}$$

Factor of 2 accounts for similar graph with internal ϕ line on lower edge

$$\begin{aligned}
&= \gamma_0 2\frac{1}{16}\gamma_0^4 \int \frac{d^dk_2 d^dk_1}{4k_1k_2}\frac{1}{i\Omega_{1n}-k_1-k_2-\lambda}\frac{1}{i\Omega_{2n}-k_2-\lambda}\frac{1}{i\Omega_{1n}-k_1-\lambda}\frac{1}{i\Omega_{1n}-k_2-\lambda} \\
&= \gamma_0 2\frac{1}{16}B_\mu\gamma^4\left(\frac{S_d}{2\widetilde{S}_{d+1}}\right)^2\left[\pi^2(-1)^{2d-6}(d-3)\csc^2(\pi d)+\frac{\pi(-1)^{2d-6}\csc(\pi d)\Gamma(6-2d)\Gamma(d-2)}{\Gamma(4-d)}\right] \\
&= \gamma_0 2\frac{1}{16}B_\mu\gamma^4\left[-\frac{1}{\epsilon}+\frac{1}{2\epsilon^2}-\frac{\aleph+2i\pi}{2\epsilon}\right], \qquad \text{(D30)}
\end{aligned}$$

$$\Gamma^{\gamma}_{13(d)} = \gamma_0 2\left(\frac{-3}{16}\right)\frac{\gamma_0^4}{\beta^2}\sum_{i\omega_{1n},i\omega_{2n}}\int d^dk_2 d^dk_1 \frac{1}{\omega_{1n}^2+k_1^2}\frac{1}{\omega_{2n}^2+k_2^2}\frac{1}{(i\Omega_{1n}+i\omega_{2n}-\lambda)^2}\frac{1}{i\Omega_{1n}+i\omega_{1n}+i\omega_{2n}-\lambda}$$
$$\times\frac{1}{i\Omega_{2n}+i\omega_{2n}-\lambda}$$

Factor of 2 is for similar graph with internal ϕ line on lower edge

$$= \gamma_0 2\left(\frac{-3}{16}\right)\gamma_0^4\int\frac{d^dk_2 d^dk_1}{4k_1k_2}\frac{1}{i\Omega_{1n}-k_1-k_2-\lambda}\frac{1}{i\Omega_{2n}-k_2-\lambda}\frac{1}{(i\Omega_{1n}-k_2-\lambda)^2}$$
$$= \gamma_0 2\left(\frac{-3}{16}\right)B_\mu\gamma^4\left(\frac{S_d}{2\widetilde{S}_{d+1}}\right)^2\left[\frac{\pi(-1)^{2d-5}\csc(\pi d)\Gamma(6-2d)\Gamma(d-1)}{\Gamma(5-d)}\right]$$
$$= \gamma_0 2\left(\frac{-3}{16}\right)B_\mu\gamma^4\left[-\frac{1}{2\epsilon^2}-\frac{-2-\aleph-2i\pi}{2\epsilon}\right], \tag{D31}$$

$$\Gamma^{\gamma}_{13(e)} = -\gamma_0 2\left(\frac{-1}{4}\right)\frac{g_0^2\gamma_0^2}{\beta^2}\sum_{i\omega_{1n},i\omega_{2n}}\int dk_2 d^dk_1\frac{|k_2|^r}{i\omega_{2n}-k_2}\frac{1}{\omega_{1n}^2+k_1^2}\frac{1}{i\Omega_{2n}+i\omega_{1n}-\lambda}\frac{1}{i\Omega_{1n}+i\omega_{1n}-i\omega_{2n}-\lambda}$$
$$\times\frac{1}{(i\Omega_{1n}+i\omega_{1n}-\lambda)^2}$$

Factor of two is for similar graph with boson line on lower edge

$$= \gamma_0 2\left(\frac{-1}{4}\right)g_0^2\gamma_0^2\int dk_2 d^dk_1\frac{|k_2|^r\theta(k_2)}{2k_1}\frac{1}{i\Omega_{1n}-k_1-k_2-\lambda}\frac{1}{i\Omega_{2n}-k_1-\lambda}\frac{1}{(i\Omega_{1n}-k_1-\lambda)^2},$$
$$= \gamma_0 2\left(\frac{-1}{4}\right)g^2\gamma^2\frac{S_d}{2\widetilde{S}_{d+1}}\left[-\frac{\pi\Gamma(d-1)\csc(\pi r)\Gamma(-d-r+4)(l-i\Omega_{1n})^{d+r-4}}{\Gamma(3-r)}\right]$$
$$= \gamma_0 2\left(\frac{-1}{4}\right)A_\mu B_\mu g^2\gamma^2\left[-\frac{1}{2\bar{r}(\epsilon+2\bar{r})}+\frac{2i\pi(\epsilon+2\bar{r})+\aleph\epsilon+2\epsilon+4\bar{r}}{4\bar{r}(\epsilon+2\bar{r})}\right], \tag{D32}$$

$$\Gamma^{\gamma}_{13(f)} = -\gamma_0 C_{sf}\frac{g_0^4}{\beta^2}\sum_{i\omega_{1n},i\omega_{2n}}\int dk_1 dk_2\frac{|k_1|^r}{i\Omega_{1n}-i\omega_{1n}-k_1}\frac{|k_2|^r}{i\omega_{2n}-k_2}\frac{1}{i\omega_{1n}-\lambda}\frac{1}{i\omega_{1n}+i\omega_{2n}-\lambda}$$
$$\times\frac{1}{i\Omega_{2n}-i\Omega_{1n}+i\omega_{1n}+i\omega_{2n}-\lambda}\frac{1}{i\Omega_{2n}-i\Omega_{1n}+i\omega_{1n}-\lambda}$$
$$= \gamma_0 C_{sf}g_0^4\int dk_1 dk_2|k_1|^r|k_2|^r\theta(k_1)\theta(-k_2)\frac{1}{i\Omega_{1n}-k_1+k_2-\lambda}\frac{1}{i\Omega_{2n}-k_1+k_2-\lambda}$$
$$\times\frac{1}{i\Omega_{1n}-k_1-\lambda}\frac{1}{i\Omega_{2n}-k_1-\lambda}$$
$$= \gamma_0 C_{sf}g^4\left[\frac{\pi r\csc(\pi r)\Gamma(2-2r)\Gamma(r+1)(l-i\Omega_{1n})^{2r-2}}{\Gamma(3-r)}\right]$$
$$= \gamma_0 C_{sf}g^4A_\mu^2\left[\frac{1}{8\bar{r}^2}-\frac{3+2i\pi}{4\bar{r}}\right]. \tag{D33}$$

We get $C_{sf}=0$. Using the results in this appendix we obtain the renormalization factors and beta

functions in Sec. III.

[1] C. Proust and L. Taillefer, "The Remarkable Underlying Ground States of Cuprate Superconductors," Annual Review of Condensed Matter Physics **10**, 409 (2019), arXiv:1807.05074 [cond-mat.supr-con].

[2] I. M. Vishik, M. Hashimoto, R.-H. He, W.-S. Lee, F. Schmitt, D. Lu, R. G. Moore, C. Zhang, W. Meevasana, T. Sasagawa, S. Uchida, K. Fujita, S. Ishida, M. Ishikado, Y. Yoshida, H. Eisaki, Z. Hussain, T. P. Devereaux, and Z.-X. Shen, "Phase competition in trisected superconducting dome," Proceedings of the National Academy of Science **109**, 18332 (2012), arXiv:1209.6514 [cond-mat.supr-con].

[3] Y. He, Y. Yin, M. Zech, A. Soumyanarayanan, M. M. Yee, T. Williams, M. C. Boyer, K. Chatterjee, W. D. Wise, I. Zeljkovic, T. Kondo, T. Takeuchi, H. Ikuta, P. Mistark, R. S. Markiewicz, A. Bansil, S. Sachdev, E. W. Hudson, and J. E. Hoffman, "Fermi Surface and Pseudogap Evolution in a Cuprate Superconductor," Science **344**, 608 (2014), arXiv:1305.2778 [cond-mat.supr-con].

[4] K. Fujita, C. K. Kim, I. Lee, J. Lee, M. H. Hamidian, I. A. Firmo, S. Mukhopadhyay, H. Eisaki, S. Uchida, M. J. Lawler, E.-A. Kim, and J. C. Davis, "Simultaneous Transitions in Cuprate Momentum-Space Topology and Electronic Symmetry Breaking," Science **344**, 612 (2014), arXiv:1403.7788 [cond-mat.supr-con].

[5] S. Badoux, W. Tabis, F. Laliberté, G. Grissonnanche, B. Vignolle, D. Vignolles, J. Béard, D. A. Bonn, W. N. Hardy, R. Liang, N. Doiron-Leyraud, L. Taillefer, and C. Proust, "Change of carrier density at the pseudogap critical point of a cuprate superconductor," Nature **531**, 210 (2016), arXiv:1511.08162 [cond-mat.supr-con].

[6] J. Loram, J. Luo, J. Cooper, W. Liang, and J. Tallon, "Evidence on the pseudogap and condensate from the electronic specific heat," Journal of Physics and Chemistry of Solids **62**, 59 (2001).

[7] J. L. Tallon, J. G. Storey, J. R. Cooper, and J. W. Loram, "Locating the pseudogap closing point in cuprate superconductors: absence of entrant or reentrant behavior," (2019), arXiv:1907.12018 [cond-mat.supr-con].

[8] B. Michon, C. Girod, S. Badoux, J. Kačmarčík, Q. Ma, M. Dragomir, H. A. Dabkowska, B. D. Gaulin, J. S. Zhou, S. Pyon, T. Takayama, H. Takagi, S. Verret, N. Doiron-Leyraud, C. Marcenat, L. Taillefer, and T. Klein, "Thermodynamic signatures of quantum criticality in cuprate superconductors," Nature **567**, 218 (2019), arXiv:1804.08502 [cond-mat.supr-con].

[9] Y. Tang, L. Mangin-Thro, A. Wildes, M. K. Chan, C. J. Dorow, J. Jeong, Y. Sidis, M. Greven, and P. Bourges, "Orientation of the intra-unit-cell magnetic moment in the high-T_c superconductor $HgBa_2CuO_{4+\delta}$," Phys. Rev. B **98**, 214418 (2018), arXiv:1805.02063 [cond-mat.supr-con].

[10] S.-D. Chen, M. Hashimoto, Y. He, D. Song, K.-J. Xu, J.-F. He, T. P. Devereaux, H. Eisaki, D.-H. Lu, J. Zaanen, and Z.-X. Shen, "Incoherent strange metal sharply bounded by a critical doping in Bi2212," Science **366**, 1099 (2019).

[11] C. Panagopoulos, J. L. Tallon, B. D. Rainford, T. Xiang, J. R. Cooper, and C. A. Scott, "Evidence for a generic quantum transition in high-T_c cuprates," Phys. Rev. B **66**, 064501 (2002), arXiv:cond-mat/0204106 [cond-mat.supr-con].

[12] C. Panagopoulos, A. P. Petrovic, A. D. Hillier, J. L. Tallon, C. A. Scott, and B. D. Rainford, "Exposing the spin-glass ground state of the nonsuperconducting $La_{2-x}Sr_xCu_{1-y}Zn_yO_4$ high-T_c oxide," Phys. Rev. B **69**, 144510 (2004), arXiv:cond-mat/0307392 [cond-mat.supr-con].

[13] M. Frachet, I. Vinograd, R. Zhou, S. Benhabib, S. Wu, H. Mayaffre, S. Krämer, S. K. Ramakrishna, A. Reyes, J. Debray, T. Kurosawa, N. Momono, M. Oda, S. Komiya, S. Ono, M. Horio, J. Chang, C. Proust, D. LeBoeuf, and M.-H. Julien, "Hidden magnetism at the pseudogap critical point of a high temperature superconductor," arXiv e-prints (2019), arXiv:1909.10258 [cond-mat.supr-con].

[14] T. Senthil, A. Vishwanath, L. Balents, S. Sachdev, and M. P. A. Fisher, "Deconfined Quantum Critical Points," Science **303**, 1490 (2004), arXiv:cond-mat/0311326 [cond-mat.str-el].

[15] S. Sachdev, N. Read, and R. Oppermann, "Quantum field theory of metallic spin glasses," Phys. Rev. B **52**, 10286 (1995), arXiv:cond-mat/9504036.

[16] A. M. Sengupta and A. Georges, "Non-Fermi-liquid behavior near a $T = 0$ spin-glass transition," Phys. Rev. B **52**, 10295 (1995), arXiv:cond-mat/9504120.

[17] J. Maldacena and D. Stanford, "Remarks on the Sachdev-Ye-Kitaev model," Phys. Rev. D **94**, 106002 (2016), arXiv:1604.07818 [hep-th].

[18] S. Sachdev and J. Ye, "Gapless spin-fluid ground state in a random quantum Heisenberg magnet," Phys. Rev. Lett. **70**, 3339 (1993), cond-mat/9212030.

[19] A. Y. Kitaev, "Talks at KITP, University of California, Santa Barbara," Entanglement in Strongly-Correlated Quantum Matter (2015).

[20] D. Mao, D. Chowdhury, and T. Senthil, "Slow scrambling and hidden integrability in a random rotor model," (2019), arXiv:1903.10499 [cond-mat.str-el].

[21] T. Senthil, S. Sachdev, and M. Vojta, "Quantum phase transitions out of the heavy Fermi liquid," Physica B Condensed Matter **359**, 9 (2005), arXiv:cond-mat/0409033 [cond-mat.str-el].

[22] P. Coleman, C. Pépin, Q. Si, and R. Ramazashvili, "Topical Review: How do Fermi liquids get heavy and die?" Journal of Physics Condensed Matter **13**, R723 (2001), arXiv:cond-mat/0105006 [cond-mat.str-el].

[23] K. Haule and G. Kotliar, "Strongly correlated superconductivity: A plaquette dynamical mean-field theory study," Phys. Rev. B **76**, 104509 (2007), arXiv:0709.0019 [cond-mat.str-el].

[24] O. Parcollet and A. Georges, "Non-Fermi-liquid regime of a doped Mott insulator," Phys. Rev. B

59, 5341 (1999), cond-mat/9806119.

[25] L. Arrachea and M. J. Rozenberg, "Infinite-range quantum random Heisenberg magnet," Phys. Rev. B **65**, 224430 (2002), cond-mat/0203537.

[26] A. Camjayi and M. J. Rozenberg, "Quantum and Thermal Fluctuations in the SU(N) Heisenberg Spin-Glass Model near the Quantum Critical Point," Phys. Rev. Lett. **90**, 217202 (2003), cond-mat/0210407.

[27] A. Georges, O. Parcollet, and S. Sachdev, "Mean Field Theory of a Quantum Heisenberg Spin Glass," Phys. Rev. Lett. **85**, 840 (2000), arXiv:cond-mat/9909239 [cond-mat.dis-nn].

[28] A. Georges, O. Parcollet, and S. Sachdev, "Quantum fluctuations of a nearly critical Heisenberg spin glass," Phys. Rev. B **63**, 134406 (2001), arXiv:cond-mat/0009388 [cond-mat.str-el].

[29] P. Werner, A. J. Kim, and S. Hoshino, "Spin-freezing and the Sachdev-Ye model," Europhys. Lett. **124**, 57002 (2018), arXiv:1805.04102 [cond-mat.str-el].

[30] N. Tsuji and P. Werner, "Out-of-time-ordered correlators of the Hubbard model: Sachdev-Ye-Kitaev strange metal in the spin-freezing crossover region," Phys. Rev. B **99**, 115132 (2019), arXiv:1812.04217 [cond-mat.str-el].

[31] P. Cha, G. Parcollet, A. Georges, and E.-A. Kim, "Incoherent metal in the quantum critical region of SU(2) symmetric model," Bull. Am. Phys. Soc. , S06.00011 (2019).

[32] P. B. Wiegmann, "Superconductivity in strongly correlated electronic systems and confinement versus deconfinement phenomenon," Phys. Rev. Lett. **60**, 821 (1988).

[33] C. Wang, A. Nahum, M. A. Metlitski, C. Xu, and T. Senthil, "Deconfined quantum critical points: symmetries and dualities," Phys. Rev. X **7**, 031051 (2017), arXiv:1703.02426 [cond-mat.str-el].

[34] A. Karch and D. Tong, "Particle-Vortex Duality from 3d Bosonization," Phys. Rev. X **6**, 031043 (2016), arXiv:1606.01893 [hep-th].

[35] E. Witten, "Global aspects of current algebra," Nucl. Phys. B **223**, 422 (1983).

[36] A. Tanaka and X. Hu, "Many-Body Spin Berry Phases Emerging from the π-Flux State: Competition between Antiferromagnetism and the Valence-Bond-Solid State," Phys. Rev. Lett. **95**, 036402 (2005), arXiv:cond-mat/0501365 [cond-mat.str-el].

[37] T. Senthil and M. P. A. Fisher, "Competing orders, nonlinear sigma models, and topological terms in quantum magnets," Phys. Rev. B **74**, 064405 (2006), arXiv:cond-mat/0510459 [cond-mat.str-el].

[38] J. Lee and S. Sachdev, "Wess-Zumino-Witten Terms in Graphene Landau Levels," Phys. Rev. Lett. **114**, 226801 (2015), arXiv:1411.5684 [cond-mat.str-el].

[39] J. L. Smith and Q. Si, "Spatial correlations in dynamical mean-field theory," Phys. Rev. B **61**, 5184 (2000), arXiv:cond-mat/9903083 [cond-mat.str-el].

[40] K. Haule, A. Rosch, J. Kroha, and P. Wölfle, "Pseudogaps in an Incoherent Metal," Phys. Rev. Lett. **89**, 236402 (2002), arXiv:cond-mat/0205347 [cond-mat.str-el].

[41] K. Haule, A. Rosch, J. Kroha, and P. Wölfle, "Pseudogaps in the t-J model: An extended dynamical mean-field theory study," Phys. Rev. B **68**, 155119 (2003), arXiv:cond-mat/0304096 [cond-mat.str-el].

[42] S. Florens and A. Georges, "Quantum impurity solvers using a slave rotor representation," Phys. Rev. B **66**, 165111 (2002), arXiv:cond-mat/0206571 [cond-mat.str-el].

[43] S. Florens and A. Georges, "Slave-rotor mean-field theories of strongly correlated systems and the Mott transition in finite dimensions," Phys. Rev. B **70**, 035114 (2004), arXiv:cond-mat/0404334 [cond-mat.str-el].

[44] S. Florens, P. Mohan, C. Janani, T. Gupta, and R. Narayanan, "Magnetic fluctuations near the Mott transition towards a spin liquid state," EPL **103**, 17002 (2013), arXiv:1006.3620 [cond-mat.str-el].

[45] W. Fu, Y. Gu, S. Sachdev, and G. Tarnopolsky, "$\mathbb{Z}_2$ fractionalized phases of a solvable, disordered, t-J model," Phys. Rev. B **98**, 075150 (2018), arXiv:1804.04130 [cond-mat.str-el].

[46] S. Sachdev, C. Buragohain, and M. Vojta, "Quantum Impurity in a Nearly Critical Two Dimensional Antiferromagnet," Science **286**, 2479 (1999), arXiv:cond-mat/0004156 [cond-mat.str-el].

[47] M. Vojta, C. Buragohain, and S. Sachdev, "Quantum impurity dynamics in two-dimensional antiferromagnets and superconductors," Phys. Rev. B **61**, 15152 (2000), arXiv:cond-mat/9912020 [cond-mat.str-el].

[48] S. Sachdev, "Static hole in a critical antiferromagnet: field-theoretic renormalization group," Physica C Superconductivity **357**, 78 (2001), arXiv:cond-mat/0011233 [cond-mat.str-el].

[49] M. Vojta and L. Fritz, "Upper critical dimension in a quantum impurity model:Critical theory of the asymmetric pseudogap Kondo problem," Phys. Rev. B **70**, 094502 (2004), arXiv:cond-mat/0309262 [cond-mat.str-el].

[50] L. Fritz and M. Vojta, "Phase transitions in the pseudogap Anderson and Kondo models: Critical dimensions, renormalization group, and local-moment criticality," Phys. Rev. B **70**, 214427 (2004), arXiv:cond-mat/0408543 [cond-mat.str-el].

[51] L. Fritz, "Quantum Phase Transitions in Models of Magnetic Impurities," Ph. D. Dissertation, Universität Karlsruhe (2006).

[52] Q. Si and G. Kotliar, "Fermi-liquid and non-Fermi-liquid phases of an extended Hubbard model in infinite dimensions," Phys. Rev. Lett. **70**, 3143 (1993).

[53] Q. Si and G. Kotliar, "Metallic non-Fermi-liquid phases of an extended Hubbard model in infinite dimensions," Phys. Rev. B **48**, 13881 (1993), arXiv:cond-mat/9307060 [cond-mat].

[54] C. Gonzalez-Buxton and K. Ingersent, "Renormalization-group study of Anderson and Kondo impurities in gapless Fermi systems," Phys. Rev. B **57**, 14254 (1998), arXiv:cond-mat/9803256 [cond-mat.str-el].

[55] A. M. Sengupta, "Spin in a fluctuating field: The Bose(+Fermi) Kondo models," Phys. Rev. B **61**,

4041 (2000).

[56] Q. Si, S. Rabello, K. Ingersent, and J. L. Smith, "Locally critical quantum phase transitions in strongly correlated metals," Nature **413**, 804 (2001), arXiv:cond-mat/0011477 [cond-mat.str-el].

[57] L. Zhu and Q. Si, "Critical local-moment fluctuations in the Bose-Fermi Kondo model," Phys. Rev. B **66**, 024426 (2002), arXiv:cond-mat/0204121 [cond-mat.str-el].

[58] J. H. Pixley, S. Kirchner, K. Ingersent, and Q. Si, "Quantum criticality in the pseudogap Bose-Fermi Anderson and Kondo models: Interplay between fermion- and boson-induced Kondo destruction," Phys. Rev. B **88**, 245111 (2013), arXiv:1306.2352 [cond-mat.str-el].

[59] Y. Huang, K. Chen, Y. Deng, and B. Svistunov, "Trapping centers at the superfluid-Mott-insulator criticality: Transition between charge-quantized states," Phys. Rev. B **94**, 220502 (2016), arXiv:1608.02232 [cond-mat.quant-gas].

[60] S. Whitsitt and S. Sachdev, "Critical behavior of an impurity at the boson superfluidMott-insulator transition," Phys. Rev. A **96**, 053620 (2017), arXiv:1709.04919 [cond-mat.quant-gas].

[61] K. Chen, Y. Huang, Y. Deng, and B. Svistunov, "Halon: A quasiparticle featuring critical charge fractionalization," Phys. Rev. B **98**, 214516 (2018), arXiv:1807.02168 [cond-mat.quant-gas].

[62] X.-Y. Song, C.-M. Jian, and L. Balents, "Strongly Correlated Metal Built from Sachdev-Ye-Kitaev Models," Phys. Rev. Lett. **119**, 216601 (2017), arXiv:1705.00117 [cond-mat.str-el].

[63] P. Zhang, "Dispersive Sachdev-Ye-Kitaev model: Band structure and quantum chaos," Phys. Rev. B **96**, 205138 (2017), arXiv:1707.09589 [cond-mat.str-el].

[64] D. Chowdhury, Y. Werman, E. Berg, and T. Senthil, "Translationally invariant non-Fermi liquid metals with critical Fermi-surfaces: Solvable models," Phys. Rev. X **8**, 031024 (2018), arXiv:1801.06178 [cond-mat.str-el].

[65] A. A. Patel, J. McGreevy, D. P. Arovas, and S. Sachdev, "Magnetotransport in a model of a disordered strange metal," Phys. Rev. X **8**, 021049 (2018), arXiv:1712.05026 [cond-mat.str-el].

[66] A. A. Patel and S. Sachdev, "Theory of a Planckian metal," Phys. Rev. Lett. **123**, 066601 (2019), arXiv:1906.03265 [cond-mat.str-el].

[67] M. Mitrano, A. A. Husain, S. Vig, A. Kogar, M. S. Rak, S. I. Rubeck, J. Schmalian, B. Uchoa, J. Schneeloch, R. Zhong, G. D. Gu, and P. Abbamonte, "Anomalous density fluctuations in a strange metal," Proceedings of the National Academy of Science **115**, 5392 (2018), arXiv:1708.01929 [cond-mat.str-el].

[68] A. A. Husain, M. Mitrano, M. S. Rak, S. I. Rubeck, B. Uchoa, J. Schneeloch, R. Zhong, G. D. Gu, and P. Abbamonte, "Crossover of Charge Fluctuations across the Strange Metal Phase Diagram," Phys. Rev. X **9**, 041062 (2019), arXiv:1903.04038 [cond-mat.str-el].

[69] B. Sutherland, "Model for a multicomponent quantum system," Phys. Rev. B **12**, 3795 (1975).

[70] P. A. Bares and G. Blatter, "Supersymmetric t-J model in one dimension: Separation of spin and

charge," Phys. Rev. Lett. **64**, 2567 (1990).

[71] S. Sarkar, "The supersymmetric t-J model in one dimension," J. Phys. A: Math. Gen. **24**, 1137 (1991).

[72] F. H. L. Essler and V. E. Korepin, "Higher conservation laws and algebraic Bethe Ansätze for the supersymmetric t-J model," Phys. Rev. B **46**, 9147 (1992).

[73] F. Göhmann and A. Seel, "A Note on the Bethe Ansatz Solution of the Supersymmetric t-J Model," Czechoslovak Journal of Physics **53**, 1041 (2003), arXiv:cond-mat/0309138 [cond-mat.str-el].

[74] S. Sachdev, H. D. Scammell, M. S. Scheurer, and G. Tarnopolsky, "Gauge theory for the cuprates near optimal doping," Phys. Rev. B **B99**, 054516 (2019), arXiv:1811.04930 [cond-mat.str-el].

[75] N. Read and S. Sachdev, "Some features of the phase diagram of the square lattice SU(N) antiferromagnet," Nucl. Phys. B **316**, 609 (1989).

[76] S. Sachdev, "Bekenstein-Hawking Entropy and Strange Metals," Phys. Rev. X **5**, 041025 (2015), arXiv:1506.05111 [hep-th].

[77] R. A. Davison, W. Fu, A. Georges, Y. Gu, K. Jensen, and S. Sachdev, "Thermoelectric transport in disordered metals without quasiparticles: The Sachdev-Ye-Kitaev models and holography," Phys. Rev. B **95**, 155131 (2017), arXiv:1612.00849 [cond-mat.str-el].

[78] Y. Gu, A. Kitaev, S. Sachdev, and G. Tarnopolsky, "Notes on the complex Sachdev-Ye-Kitaev model," (2019), arXiv:1910.14099 [hep-th].